Infrared luminescence of chalcogenide glasses doped with rare earth ions and their potential applications

V. Nazabal, J.-L. Adam

Infrared luminescence of chalcogenide glasses doped with rare-earth ions and their potential applications

Abstract

This article deals with sulfur and selenium-based glasses doped with rare-earth ions. It reviews the most significant glass compositions and their related thermal and mechanical properties, with emphasis given to optical and spectroscopic properties in the infrared domain. Optical transparency, multiphonon relaxations, luminescence in optical fibers and planar waveguides doped with trivalent rare-earth ions are presented in details. Applications as new compact light sources and lasers, especially for the mid-IR domain, are shown.

Keywords (6)

Photoluminescence; mid-infrared; low-phonon glasses; optical fibers; thin film; photonic integrated circuit

1 Introduction

Chalcogenide glasses possess unique optical properties and very good ability to be manufactured in a broad range of optical objects, like lenses, fibers,thin films, photonic integrated circuit (PIC). The main optical properties, which differentiate chalcogenide glasses from their oxide or fluoride counterparts, are i) the intrinsic broad infrared transparency that may extend up to 25 µm with tellurium-rich glasses, ii) the high quantum efficiency of rare-earth ions emission, which results in luminescence at wavelengths not accessible with other glasses, especially in the mid-infrared (mid-IR), iii) the high non-linear refractive indices, which allow the occurrence of efficient non-linear phenomena by using lower incident powers or shorter lengths of light-matter interaction compared to oxide and fluorides glasses.

This article deals with sulfur and selenium -based glasses doped with rare-earth ions, reviewing the most significant glass compositions and their related thermal and mechanical properties, with emphasis given to optical and spectroscopic properties in the infrared domain. Optical transparency, multiphonon relaxations, luminescence in optical fibers and planar waveguides doped with trivalent rare-earths ions are reviewed. Applications as new compact light sources and lasers, especially for the mid-IR domain, are shown.

2 Basics of chalcogenide glasses

2.1 Glass compositions and their fundamental properties

Chalcogenide glasses refer to glassy materials based on S, Se, or Te, possibly associated to nearby elements of the periodic table such as Ge, As, Ga, Sb, and halides. Addition of these elements results in glasses with improved stability against crystallization. The most stable glasses can be fabricated in the form of lenses by molding, of optical fibers by drawing, and of thin films by various techniques including chemical and physical vapor deposition. Details on glass synthesis and fabrication can be found in [1].

Up to now, rare-earth spectroscopy has been studied in sulfide and selenide glasses only. These glasses show reasonably easy conditions for incorporating rare-earth ions and an appropriate position of the bandgap for pumping with available light sources, contrary to

telluride glasses. Incorporating rare-earth ions in Ge-based sulfide glass matrix is facilitated in presence of Ga, leading to glasses with higher rare-earth content and less clustering. Due to the lower charge of Ga relative to Ge, electron donors such as rare-earth dopants act as charge-balancing cations for $GaS_{4/2}$ tetrahedra, offering preferred crystallographic sites for rare-earth ions [2]. Examples are Ge-Ga-Sb-S/Se glasses, whose physical properties are displayed in **Erreur ! Source du renvoi introuvable.**. Ga-La-S glass, which corresponds to 70 Ga_2S_3 – 30 La_2S_3 formulation, is a special case where lanthanum sulfide is one of the glass constituents. Substitution of an active rare-earth for La is then straightforward.
The presence of four-fold coordinated elements like germanium and gallium aims at increasing the reticulation within the glass This results in increasing glass transition temperatures, T_g, from As_2S_3 to Ge-based glasses and Ga-La-S glass, whose T_g is as high as 553 °C, as shown in Table 1. Logically, thermal expansion coefficients evolve in the opposite way, decreasing with the reticulation of the network. For Ga-la-S, it is as low as 6.04 10^{-6} K^{-1}. For comparison, the glass transition temperature and thermal expansion coefficient of silica are equal to 1200 °C and 0.5 10^{-6} K^{-1}, respectively.

Table 1 : Properties of some chalcogenide glass compositions suitable for rare-earth doping

Glass composition	Glass transition temperature (°C)	Thermal expansion coefficient (10^{-6} K^{-1})	Density (g cm^{-1})	Refractive index	Reference
$Ge_{20}Ga_5Sb_{10}S_{65}$	297	15.1	3.2	2.3657 @ 632 nm 2.2514 @ 1.55 µm 2.220 @ 4µm	[3] [4] [5]
70 Ga_2S_3 – 30 La_2S_3	553	6.04	4.11	2.37 @ 1.5 µm	[6], [7]
As_2S_3	182	22.5	3.2	2.4375 @ 1.55 µm 2.4202 @ 3 µm	[8]
$Ge_{25}Ga_5Sb_{10}Se_{60}$	283	15.5	4.69	2.6709 @ 2 µm	[9]
$Ge_{33}As_{12}Se_{55}$	368	12.1	-	2.5450 @ 1.55 µm 2.5146 @ 4 µm	[9] [1]

2.2 Optical properties

Optical properties are the features that best identify chalcogenide glasses among the various families of glasses. First, they show a broad transparency in the mid-infrared spectral domain. This is directly related to the low frequency of fundamental vibration modes of chalcogenide matrices, which allows transmission of light at wavelengths up to of 10 µm for sulfides, and above 20 µm for tellurium-rich glasses. These low-frequency vibrations result also in lower probabilities for non-radiative relaxations in rare-earth-doped chalcogenide glasses, hence increasing the quantum efficiency of the luminescence of rare-earth ions in such hosts. High linear refractive indices (> 2.2, as shown in Table 1) and, consequently, large nonlinear refractive indices, which are 2 to 3 orders of magnitude higher than that of silica, are also specific features of chalcogenide glasses, as described in [11].

Optical transmission is probably the one optical parameter that best characterizes chalcogenide glasses. Indeed, their ability to transmit mid-IR light has been known for decades [12]. Figure 1 shows the infrared edge of some typical glass families. Silica glass transmits light up to 3 µm only for a thickness of a few millimeters. This limitation is related to the high frequency of intrinsic fundamental vibration modes due to stretching of Si – O bonds, which are around 1100 cm^{-1}. In fluoride glasses, the infrared edge is located at longer

wavelengths, around 7 µm. This is because vibrations modes are at much lower frequencies, as compared to oxides. In fluorozirconate glasses for instance, the fundamental Zr – F vibration in ZrF_n polyhedra is equal to 570 cm^{-1}.

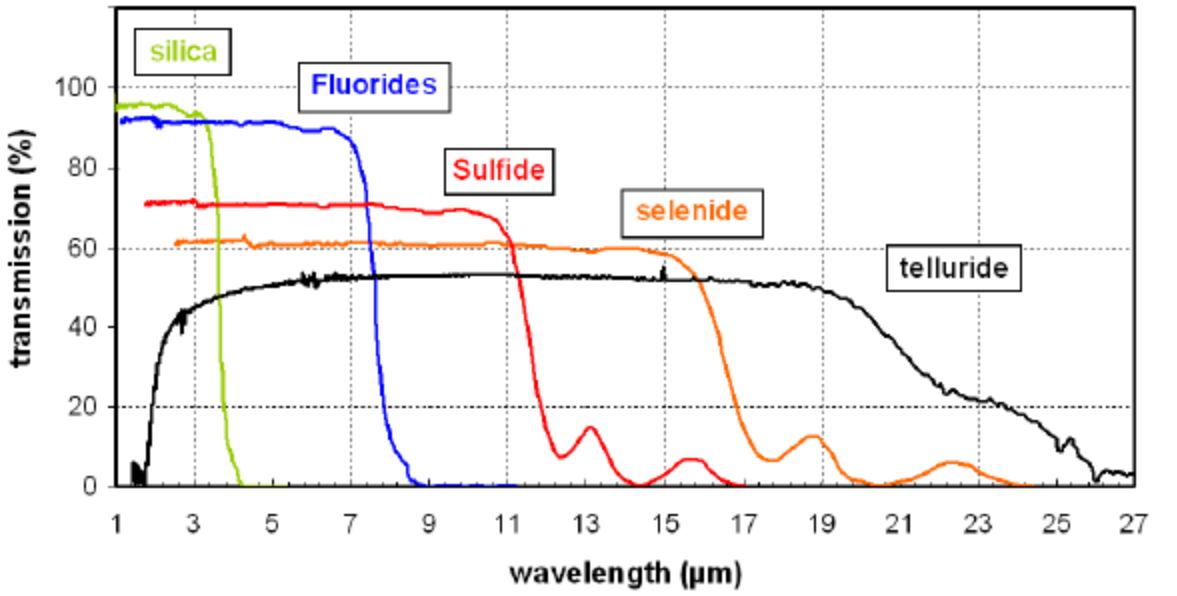

Figure 1 : Infrared optical transmission of silica, fluoride and chalcogenide glasses (from [1])

In chalcogenides, which contain heavier chemical elements and have a weaker chemical bond strength, the main fundamental vibration modes are located at even lower frequencies, typically at 340 cm^{-1} in sulfide glasses where Ge and S are the main constituents, and at 200 cm^{-1} in Ge-Se selenide glasses considering Raman scattering spectroscopy and stoichiometric composition. In non-stoichiometric glasses, the stretching vibration modes are observable up to higher energy and the antisymmetric stretching modes observable by IR spectroscopy are also at higher energy than symmetric stretching modes [13], [14], [15]. Consequently, the main energy of phonons can be considerated in a range for sulfide glasses of 300-475 cm^{-1}, 200-300 cm^{-1} for selenides and 130-220 cm^{-1} for telluride glasses.These low frequencies are responsible for the shift towards longer wavelengths of the infrared edge due to multiphonon absorption, in the series S < Se < Te.

In the short-wavelength region, the optical transmission is limited by electronic transitions between the non-bridging energy band due to the lone pairs of p electrons of chalcogenide elements, and the conduction band corresponding to anti-bonding levels [16]. Optical band gaps in chalcogenide glasses, defined as the onset of absorption edge due to electronic transitions, decrease in the series S > Se > Te. As a result, sulfide glasses, which exhibit the largest band gap, are partially transparent in the visible and show a red color. With optical band gaps below 1.8 eV, selenide and telluride glasses are not transparent in the visible and show a characteristic black color with a shiny aspect. This visual property is due to the high refractive index of selenides and tellurides, as shown in Table 1 for selenides, which induces high reflectivity and consequently a maximum transmission of nearly 60 % in the transparency domains (Figure 1). The optical band gap can be shifted significantly towards shorter wavelengths by adding elements such as Cl atoms, whose electronegative nature permits to better localize the lone pair of p electrons of chalcogenides [16].

The intrinsic transparency of chalcogenide glasses can be altered by the presence of impurities. These impurities are essentially H, O and C that can be present in the raw materials or incorporated during the synthesis process if great care is not taken to isolate the batch from the atmosphere. When the impurities (X) are bonded to the glass components (M), then extrinsic M-X vibration modes are present in the glass, resulting in the absorption of light at specific wavelengths, as detailed in [17], [18]. Water in the molecular state is also responsible for absorption of light in chalcogenides.

3 Spectroscopy of chalcogenide glasses doped with rare-earth ions

As described in §.2.2, chalcogenide glasses are characterized by intrinsic low-energy phonons responsible for the broad transparency window in the mid-IR. Low-energy phonons are also responsible for the low probabilities of non-radiative relaxations in chalcogenide glasses. Then, the luminescence of rare-earth ions (RE) exhibits enhanced quantum efficiencies. Rare-earth-doped chalcogenide glasses possess a high potential for generating light at wavelengths where rare-earth-doped oxide glasses cannot operate, especially in the mid-IR domain. A comprehensive review is available in [19].

3.1 Multiphonon relaxations

While the measurement of multiphonon emission rates is quite straightforward in glasses transparent in the visible, like oxides [20] or fluorides [21], [22], [23], the situation is more complex in chalcogenides, because of the poor transparency in the visible that limits the number of energy levels available for the measurement. For this reason, only sulfide glasses have been investigated for measuring multiphonon emission rates.

For a given energy level of a trivalent rare earth ion, and at a given temperature, the multiphonon emission rate (W_{MP}) is expressed by the "energy-gap law":

$$W_{MP} = C \exp(-\alpha \Delta E) \qquad \text{Equation 1}$$

Where C (s^{-1}) and α (cm) are positive constants characteristic of the host, and ΔE (cm^{-1}) is the energy gap between the emitting level and the next lower-lying level. The results obtained for various sulfide glasses are shown in

Table 2.

Table 2 : Non-radiative parameters of rare-earth transitions in sulfide glasses at room temperature

Glass	C (10^6 s^{-1})	α (10^{-3} cm)	Phonon energy (cm^{-1})	Reference
$Ge_{20}Ga_5Sb_{10}S_{65}$ ($\Delta E < 2500$ cm^{-1})	3800	6.6	350	[24]
$Ge_{20}Ga_5Sb_{10}S_{65}$ ($\Delta E > 2500$ cm^{-1})	1	2.1	350	[24]
$Ge_{25}Ga_{1.67}As_{8.33}S_{65}$ ($\Delta E < 2600$ cm^{-1})	3800	6.7	425	[25]
$Ga_{37.5}La_{12.5}S_{50}$ ($\Delta E < 2300$ cm^{-1})	1	2.9	350	[26]
$Ge_{30}As_{10}S_{60}$ ($\Delta E < 3500$ cm^{-1})	0.8	2.8	350	[27]
$Ge_{25}Ga_5S_{70}$ ($\Delta E < 3500$ cm^{-1})	2.6	2.9	350	[27]

In chalcogenides, for energy levels where the energy gap is greater than 2500 cm^{-1}, results must be taken with care because multiphonon relaxations may not be the predominant mechanisms involved in the decay from those levels. Indeed, the apparently large multiphonon emission rate observed for $\Delta E > 2500$ cm^{-1} is explained as being due to a strong contribution of diffusion-limited relaxation process to the OH or SH impurities contained in the glass [24]. Introduction of heavier elements such as Cs and Br into GeGaS glass results in a significant decrease of the multiphonon relaxation rate [28].

In any case, multiphonon relaxations are less probable in chalcogenide glasses than in oxide glasses, by several orders of magnitude. As an illustration, multiphonon rates are in the range of 10^4 s^{-1} in chalcogenides and 10^8 s^{-1} in silicates, for an energy gap of 2000 cm^{-1} [20].

3.2 Emission properties

Rare-earth-doped chalcogenide glasses are of high interest for light emission in the mid-IR domain. The spectral profiles of optical transitions specific of chalcogenides are shown in Figure 2.

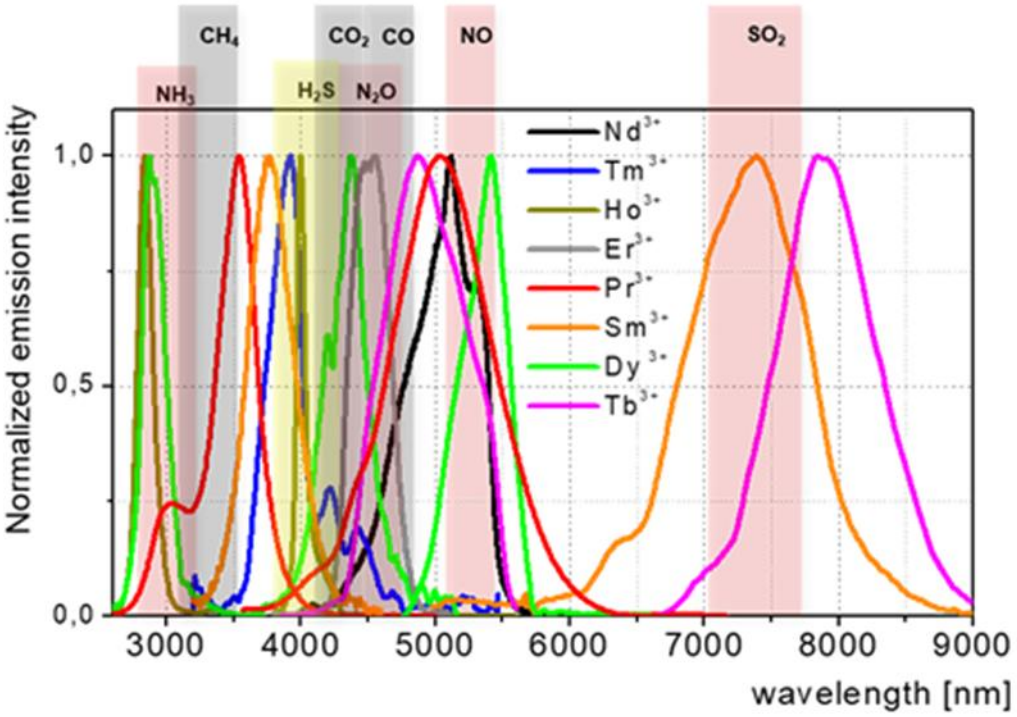

Figure 2 : Spectral profiles of infrared emissions in rare-earth-doped chalcogenide glasses, and absorption domains of some molecules having detrimental effects on environment and health.

Considering the full-width at half-maximum (FWHM) of the emission bands, rare-earth-doped chalcogenide glasses cover the 2.5 – 8.4 µm mid-IR spectral range, except around 3.2 µm and between 5.7 and 6.7 µm. This opens new possibilities for designing infrared optical devices like fiber or planar optical sensors capable to detect molecules whose vibration modes are resonant with the light emitted from rare-earth-doped chalcogenide glasses. In this matter, molecules with detrimental effects on environment and health, like greenhouse effect gases (CO_2, CH_4, N_2O) and air pollutants (SO_2, H_2S, etc.) are of specific interest.
The relevant spectroscopic properties of infrared emissions of rare-earth ions in various chalcogenide glasses are shown in

Table 3. The few emissions that occur in the visible domain with rare-earth-doped sulfide and halo-sulfide glasses are not listed here. In addition, rare-earth-doped chalcogenide glass-ceramics are treated elsewhere [29].

Table 3 : Spectroscopic properties of mid-IR emissions in rare-earth-doped sulfide and selenide glasses. A_{ed} : electric-dipole emission rate ; τ: (1) radiative lifetime, (2) experimental lifetime at room temperature, (3) experimental lifetime at low temperature; β: branching ratio; η : quantum efficiency. (♦) Quantum efficiencies weighted by branching ratios. (*) Transitions observed in optical fibers.

RE ion	Transition	Glass	λ (μm)	τ (μs)	β	η (%)	Ref.
Ce^{3+}	$^2F_{7/2} \rightarrow {}^2F_{5/2}$	$Ge_{20}Ga_5Sb_{10}Se_{65}$	3.5 - 6	1330 (2)	1	-	[30]
Pr^{3+}	$^1G_4 \rightarrow {}^3H_5$	Ga-La-S	1.3	295 (2)	0.52	58	[31]
		Ga-Na-S		370 (2)	0.52	58	
		Ge-S	1.34	358 (2)	-	90	[32]
		Ge-As-S	1.34	-	-	-	[2]
		Ga-Ge-As-S		-	-	-	
	$^1G_4 \rightarrow {}^3H_5$	Ba-In-Ga-Ge-Se	1.35	250 (1)	0.620	70	[33]
	$^3F_3, {}^3F_4 \rightarrow {}^3H_4$		1.6	230 (1)	0.766, 0.627	40	
	$^1G_4 \rightarrow {}^3H_6, {}^3F_2$		1.7 - 2.6	-	-	-	
	$^3F_3, {}^3F_4 \rightarrow {}^3H_5$			-	-	-	
	$^3H_6, {}^3F_2 \rightarrow {}^3H_4$			5200 (1)	-	6	
	$^1G_4 \rightarrow {}^3F_4, {}^3F_3$		3 - 5.5	-	-	-	
	$^3F_4 \rightarrow {}^3F_2$			-	-	-	
	$^3F_4, {}^3F_3 \rightarrow {}^3H_6$			-	-	-	
	$^3H_6, {}^3F_2 \rightarrow {}^3H_5$			-	-	-	
	$^3H_5 \rightarrow {}^3H_4$			12 900 (1)	1	20	
	$^3F_3 \rightarrow {}^3H_4$	$Ge_{36}Ga_5Se_{59}$	1.68	241 (1), 135 (2)	0.74	-	[34]
	$^3F_3, {}^3F_4 \rightarrow {}^3H_5$		2 - 2.7	241(1), 424(1)	0.247, 0.242	-	
	$^3F_2, {}^3H_6 \rightarrow {}^3H_4$			356(1), 5210(1)	0.906, 0.530	-	
	$^3F_2 \rightarrow {}^3H_5$		3.4	356 (1)	0.094	-	
	$^3F_3, {}^3F_4 \rightarrow {}^3H_6$		3.9 - 5.4	241(1), 424(1)	0.013, 0.067	-	
	$^3F_4 \rightarrow {}^3F_2$			424(1)	0.002	-	
	$^3H_5 \rightarrow {}^3H_4$			11200 (1), 8500 (2)	1.000	-	
	$^3F_3 \rightarrow {}^3F_2$		7.2	241 (1), 135 (2)	0.00078	-	
	$^1G_4 \rightarrow {}^3F_4$	Ge-As-Ga-Se	3.4	360 (1) 220 (2)	0.043	61	[35]
	$^3H_6, {}^3F_2 \rightarrow {}^3H_5$		3.9	3400 (1) 4200 (2)	0.420	100	
	$^3H_5 \rightarrow {}^3H_4$		4.8	15000 (1), 12000 (2)	1.000	80	
				7800 (2)	1.000	-	[36]
Nd^{3+}	$^4F_{3/2} \rightarrow {}^4I_{9/2}$	Ga-La-S	0.92	-	-	-	[37]
	$^4F_{3/2} \rightarrow {}^4I_{11/2}$		1.1	-	-	-	
	$^4F_{3/2} \rightarrow {}^4I_{13/2}$		1.36	-	-	-	
		$Ge_{20}Ga_5Sb_{10}S_{65}$	0.96	70 (1)	0.55	-	[5]
			1.095	70 (1)	0.39	-	
			1.387	70 (1)	0.06	-	
	$^4I_{13/2} \rightarrow {}^4I_{11/2}$		4.2 – 5.7 (*)	9670 (1)	0.33	-	
	$^4I_{15/2} \rightarrow {}^4I_{13/2}$			8520 (1)	0.30	-	
	$^4I_{11/2} \rightarrow {}^4I_{9/2}$			31040 (1)	1.00	-	
Sm^{3+}	$^6F_{11/2} \rightarrow {}^6H_{7/2}$	Ge-Ga-Se	1.08	92 (1)	0.13	-	[38]
	$^6F_{11/2} \rightarrow {}^6H_{9/2}$		1.24	92 (1)	0.23	-	
	$^6F_{11/2} \rightarrow {}^6H_{11/2}$		1.49	92 (1)	0.27	-	
	$^6F_{5/2,3/2,1/2}, {}^6H_{15/2} \rightarrow {}^6H_{5/2}$	$Ge_{20}Ga_5Sb_{10}Se_{65}$	1.65 (*)	390 (1)	0.39	-	[39]
	$^6H_{13/2} \rightarrow {}^6H_{5/2}$		1.95 (*)	4340 (1)	0.17	-	
	$^6H_{13/2} \rightarrow {}^6H_{9/2}$		3.7 (*)	4340 (1)	0.33	-	
	$^6H_{13/2} \rightarrow {}^6H_{11/2}$		7.2 (*)	4340 (1)	0.08	-	
	$^6H_{13/2} \rightarrow {}^6H_{7/2}$	$Ge_{19.4}Ga_3Sb_{9.7}Se_{67.9}$	2.70 (*)	-	-	-	[40]
	$^6H_{13/2} \rightarrow {}^6H_{9/2}$		3.75 (*)	100 (2)	-	-	
	$^6H_{13/2} \rightarrow {}^6H_{11/2}$		7.25 (*)	100 (2)	-	-	

Tb^{3+}	$^7F_4 \rightarrow {}^7F_6$ $^7F_5 \rightarrow {}^7F_6$ $^7F_4 \rightarrow {}^7F_5$	Ge-As-Ga-Se	3.2 4.8 7.5	8000 [1], 12 [2] 15000[1] , 11000[2] 8000 [1], 12 [2]	0.88 1.00 0.12	0.15 73 0.15	[35]
		$Ge_{20}Ga_5Sb_{10}Se_{65}$	3.1 [*] 5.0 [*] 8.0 [*]	4900 [1] 13900[1], 8900[2] 4900 [1]	0.93 1.00 0.07	- 64 -	[41]
	$^7F_5 \rightarrow {}^7F_6$	Ge-As-Ga-Se	4.8	12900 [2]	1	-	[42]
		Ga-La-S	4.8	16700 [1], 100 [2]	1	0.6	[43]
Dy^{3+}	$^6F_{9/2}$, $^6H_{7/2} \rightarrow {}^6H_{15/2}$ $^6F_{11/2}$, $^6H_{9/2} \rightarrow {}^6H_{15/2}$ $^6F_{9/2}$, $^6H_{7/2} \rightarrow {}^6H_{9/2}$, $^6F_{11/2}$	$Ge_{20}Ga_5Sb_{10}Se_{65}$	1.15 [*] 1.38 [*] 7.3 [*]	130 [1], 42 [2] 230 [2] 130 [1], 42 [2]	0.650 0.910 0.004	32 - 32	[44]
	$^6F_{11/2}$, $^6H_{9/2} \rightarrow {}^6H_{15/2}$	Ga-La-S Ge-As-Se	1.3	59 [2] 310 [2]	0.93 0.93	29 95	[31]
		$Ge_{20}Ga_5Sb_{10}S_{65}$	1.34	379 [1]	0.907	10	[45]
		$Ge_{20}Ga_5Sb_{10}S_{65}$	1.35	190 [1]	0.908	-	[46]
	$^6H_{11/2} \rightarrow {}^6H_{15/2}$ $^6H_{13/2} \rightarrow {}^6H_{15/2}$ $^6H_{11/2} \rightarrow {}^6H_{13/2}$	$Ge_{20}Ga_5Sb_{10}S_{65}$	1.76 2.87 4.35	2310 [1] 7030 [1] 2310 [1]	0.912 1.000 0.088	- - -	
		$Ga_8Sb_{32}S_{60}$	1.79 2.95 4.4	1870 [1], 1440 [2] 4110 [1] , 3620 [2] 1870 [1] , 1420 [2]	0.860 1.000 0.140	76 88 76	[47]
		Ge-Ga-S	1.79 2.95 4.4	3170 [1], 1310 [2] 6990 [1] , 3530 [2] 3170 [1] , 1320 [2]	0.86 1.00 0.14	41 50 41	
	$^6H_{13/2} \rightarrow {}^6H_{15/2}$ $^6H_{11/2} \rightarrow {}^6H_{13/2}$	Ga-La-S	2.83 4.27	6290 [1], 3600 [2] 2530 [1], 1300 [2]	1.00 0.14	57 51	[48], [49]
	$^6H_{13/2} \rightarrow {}^6H_{15/2}$ $^6H_{11/2} \rightarrow {}^6H_{13/2}$	Ga-Sb-La -S	2.95 4.40	3900 [1], 2920 [2] 1820 [1], 1260 [2]	1.00 0.14	75 69	[50]
		Ge-As-Ga-Se	3.0 4.5	6200 [1], 6000 [2] 2400 [1] , 2000 [2]	1.00 0.10	97 83	[35]
		$Ga_8Sb_{32}S_{55}I_5$	2.92 4.41	3150 [1], 2820 [2] 1460 [1], 1190 [2]	1.00 0.15	90 82	[51]
Ho^{3+}	$^5I_7 \rightarrow {}^5I_8$	As_2S_3	2.01	-	-	-	[52]
	$^5I_7 \rightarrow {}^5I_8$ $^5I_6 \rightarrow {}^5I_7$	$Ge_{30}As_{10}S_{60}$	2.0 2.9	5640 [1] 2180 [1]	1.000 0.109	- -	[53]
		$Ge_{20}Ga_5Sb_{10}S_{65}$	1.96 2.91	9170 [1] 7420 [1]	1.000 0.348	- -	[54]
Er^{3+}	$^4I_{13/2} \rightarrow {}^4I_{15/2}$ $^4I_{11/2} \rightarrow {}^4I_{13/2}$	Ga-La-S	1.54 2.75	2030 [1], 2300 [2] 1530 [1], 1230 [2]	1.00 0.14	- 80	[55]
		$Ge_{20}Ga_5Sb_{10}S_{65}$	1.53 2.77	1800 [1], 1900 [2] 1400 [1,2]	1.000 0.138	100 100	[56]
	$^4I_{9/2} \rightarrow {}^4I_{11/2}$		4.3 – 4.7	1100 [1], 700 [2]	0.008	64	
Tm^{3+}	$^3H_5 \rightarrow {}^3H_6$ $^3H_4 \rightarrow {}^3F_4$ $^3F_4 \rightarrow {}^3H_6$	$Ge_{20}Ga_5Sb_{10}S_{65}$	1.20 1.47 1.80	760 [3] 155 [3] 1300 [3]	0.99 0.08 1.00	- - -	[57], [58]
	$^3H_5 \rightarrow {}^3H_6$ $^3H_4 \rightarrow {}^3F_4$ $^3F_4 \rightarrow {}^3H_6$	$Ga_{0.8}As_{39.2}S_{60}$	1.22 1.46 1.82	500 [2] 116 [2] -	- - -	- - -	[59]
	$^3H_5 \rightarrow {}^3H_6$ $^3H_4 \rightarrow {}^3F_4$	$Ga_{25}Ga_5S_{70}$	1.21 1.45 1.81 2.35	683 [1] 163 [1] 978 [1] 163 [1]	0.90 0.09 1.00 0.02	- - -	[27]
	$^3F_4 \rightarrow {}^3H_6$ $^3H_4 \rightarrow {}^3H_5$	Ga-La-S	1.22 1.47 1.83 2.35	760 [1] , 730 [2] 158 [1] , 220 [2] 970 [1] , 1160 [2] 158 [1] , 220 [2]	0.97 0.08 1.00 0.02	93 [♦] 8 [♦] 100 [♦] 2 [♦]	[43]
	$^3H_5 \rightarrow {}^3F_4$		3.88	760 [1] , 730 [2]	0.03	3 [♦]	
Yb^{3+}	$^2F_{5/2} \rightarrow {}^2F_{7/2}$	Ge-Ga-S-CsBr	≈ 1.00	440 [1], 770 [2]	-	100	[28]

Several studies have been devoted in the past to Pr^{3+}- and Dy^{3+}-doped sulfide and selenide glasses as potential optical fiber amplifiers around 1.3 µm, in the so-called O-band in telecommunication (1.26 - 1.36 µm). Figure 3 shows the broad emission band of Dy^{3+} in $Ge_{20}Ga_5Sb_{10}S_{65}$ peaking at 1.34 µm with a full-width at half-maximum (FWHM) of 95 nm covering a large part of the O-band [45]. With Pr^{3+}, optical amplification was demonstrated in a Ga-Na-S glass fiber. A high net gain of 32 dB was obtained with pump power of 90 mW at 1.02 µm [60].

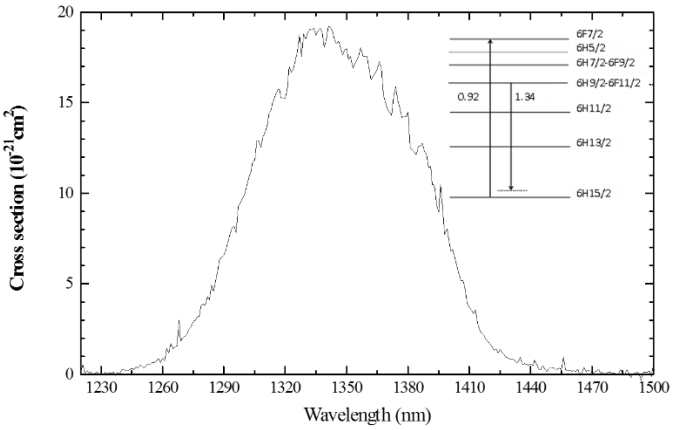

Figure 3 : 1.34-µm emission spectrum of Dy^{3+} ions in $Ge_{20}Ga_5Sb_{10}S_{65}$ glass [45]

In the near infrared, laser action was obtained in bulk configuration, at 1 µm with a Nd^{3+}-doped Ga-La-S chalcogenide glass [37]. The threshold was less than 10 mW, for a maximum output power of 2.7 mW and a slope efficiency of 11%.

Transitions at nearly 1.5 µm ($^4I_{13/2} \rightarrow {}^4I_{15/2}$) and 2.7 µm ($^4I_{11/2} \rightarrow {}^4I_{13/2}$) were observed in Er^{3+}-doped GaLaS and $Ge_{20}Ga_5Sb_{10}S_{65}$ sulfide glasses [55], [56]. In $Ge_{20}Ga_5Sb_{10}S_{65}$, fluorescence decays were found to be single exponential in nature for Er^{3+} concentration of 500 ppm, indicating the absence of energy transfer for that low concentration. In addition it was shown that lifetimes were constant in these high-purity glasses, provided that the SH content does not exceed 95 ppm. This demonstrates that extrinsic multiphonon relaxations due to SH impurities are negligible. The absence of both energy transfer and multiphonon relaxations in these high-purity, low rare-earth content glasses is confirmed by the good agreement between radiative and experimental lifetimes, leading to quantum efficiencies of 100 % for both transitions. Broad luminescence centered at 2.77 µm was measured in Er^{3+}-doped $Ge_{20}Ga_5Sb_{10}S_{65}$ planar channel waveguides, as well as an on/off gain at 1.54 µm [61]. At that same wavelength (1.54 µm), an internal gain was demonstrated in As_2S_3 channel waveguides [62]. In GaLaS glass, lifetimes are in the same order of magnitude as in $Ge_{20}Ga_5Sb_{10}S_{65}$. The highest value obtained for the measured lifetime of the $^4I_{13/2}$ level, as compared to the radiative one, can be attributed to radiative reabsorption and reemission at 1.5-µm [63].

In the 2-3 µm region, Ho^{3+} possesses two transitions of interest: $^5I_7 \rightarrow {}^5I_8$ emitting at 2 µm (eye-safe wavelength, belongs to an atmosphere-transparent domain), and $^5I_6 \rightarrow {}^5I_7$ at 2.9 µm (resonance with vibration modes of water molecules). The radiative lifetimes shown in

Table 3 differ significantly between the two types of glasses, even though they are quite similar in terms of chemical formulation. These discrepancies can be attributed to poor conditions for applying the Judd-Ofelt theory to Ho^{3+}-doped chalcogenide glasses, leading to potentially significant errors in the calculation. Because of the limited transparency of chalcogenides in the visible, only four absorption bands are taken into account for determining the three Judd-Ofelt parameters. This is the minimum number of transitions required for implementing the least squares fitting procedure in Judd-Ofelt calculations. A theoretical study demonstrated the potential of Ho^{3+}-doped $Ge_{20}Ga_5Sb_{10}S_{65}$ glasses by predicting a high gain of nearly 35 dB in a 15-meter fiber amplifier [54].

Tm^{3+} ions exhibit several emissions in the 1-3 µm range, as shown in

Table 3. Main features are the 1.2 µm emission from the $^3H_5$ level, which can be observed in low-phonon energy materials only, the 1.45 µm transition from $^3H_4$ to $^3F_4$, which corresponds to the S-Band in telecommunication (1.46 – 1.53 µm), and the 1.8 µm transition from the first excited state to the ground level, which belongs to an eye-safe spectral region. Emission at 3.88 µm from $^3H_5$ to $^3F_4$ is observed in GaLaS glass [43].

Emissions at wavelengths around 3 µm and above have been achieved in both sulfide and selenide glasses, several of them with quantum efficiencies as high as 80 % and more. These transitions are of interest as sources for the 3-5 µm transparency window of the atmosphere, or for optical sensing of molecules that show specific fingerprints in that spectral region. Thus, the broad 4.4 µm emission (FWHM=300 nm) of Dy^{3+}, displayed in Figure 4, has been successfully utilized to perform quantitative detection of CO_2 gas [64] [65], as described further in §.4.1. Er^{3+} ions possess also a transition that coincides with CO_2 absorption. That transition is from $^4I_{9/2}$ to the $^4I_{11/2}$ level and peaks at 4.6 µm, spanning the 4.3 - 4.8 µm spectral band [56].

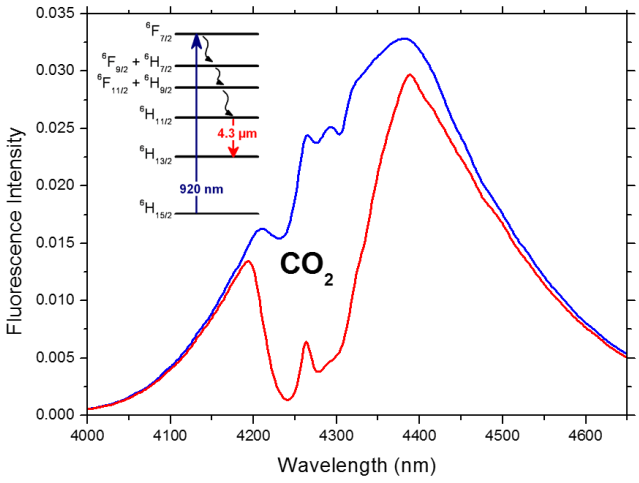

Figure 4 : Fluorescence spectrum around 4.4 µm of a Dy^{3+}-doped $Ge_{20}Ga_5Sb_{10}S_{65}$ single-index glass fiber under excitation at 920 nm, modified by the presence of CO_2 gas [64]

In that same spectral region, the combination of Pr^{3+} transitions at 3.9 and 4.8 µm leads to a super-broad band spanning from 3.5 to 5.5 µm in $Ge_{20}Ga_5Sb_{10}S_{65}$ bulk glass and single-index fiber, as shown if Figure 5 [66]. A similar band profile is recorded with Ge-As-Ga-Se small-core double-index fiber [67].

Nd^{3+} ions exhibit a super-broad band as well, from 4.2 to 5.7 µm, due to transitions from the $^4I_{15/2}$, $^4I_{13/2}$, and $^4I_{11/2}$ lower-lying levels. This was observed in $Ge_{20}Ga_5Sb_{10}S_{65}$ single-index fiber [5].
Recently, broad emission from Ce^{3+} ions was reported in $Ge_{20}Ga_5Sb_{10}Se_{65}$ selenide glass [30]. Attributed to the $^2F_{7/2} \rightarrow {}^2F_{5/2}$ transition, this emission covers the 3.5 – 6 µm spectral range with a maximum peaking at around 4.5 µm and a measured lifetime of 1.33 ms.

Fluorescence Signal (a.

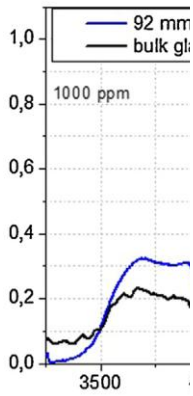

Wavelength (nm)

Figure 5 : Ultra-broad fluorescence spectra of 1000 ppm Pr^{3+}-doped $Ge_{20}Ga_5Sb_{10}S_{65}$ single-index fiber and bulk glass due to the ($^3F_2$,$^3H_6$) → $^3H_5$ (3.5 – 4.2 µm) and $^3H_5$→$^3H_4$ (4.0 – 5.5 µm) transitions [66].

Luminescence has been observed at wavelengths greater than 6 µm in rare-earth-doped selenide glass fibers. The transitions involved are, namely, $^6H_{13/2}$ → $^6H_{11/2}$ of Sm^{3+}, $^7F_4$ → $^7F_5$ of Tb^{3+}, and $^6F_{9/2}$, $^6H_{7/2}$ → $^6H_{9/2}$, $^6F_{11/2}$ of Dy^{3+}, whose spectroscopic data are given in

Table 3 for various types of Ge-Se based glasses. Emission profiles of $Ge_{20}Ga_5Sb_{10}Se_{65}$ fibers doped with 1000-ppm rare-earth ions are plotted in Figure 6. These transitions are in strong competition with multiphonon relaxations, so that they take place in selenide glasses only, not in sulfide. Multiphonon relaxations are significantly less probable in selenides, with Ge-Se fundamental vibration modes equal to 220 cm^{-1}, as compared to sulfide glasses where Ge-S fundamental modes are at 340 cm^{-1}. However, even in selenides, quantum efficiencies may remain at a low level (e.g. 0.15 % for the $^7F_4 \rightarrow {}^7F_5$ transition of Tb^{3+}in Ge-As-Ga-Se glass [35]). In addition, these transitions exhibit very low branching ratios. As a result, their observation requires an optical fiber configuration in order to take advantage of better pumping conditions like light coupling and confinement, together with longer distances of interaction between light and matter. Altogether, the most intense emission is obtained at 7.2 µm with a 100-mm long fiber doped with 1000 ppm Sm^{3+}, as shown in Figure 6.

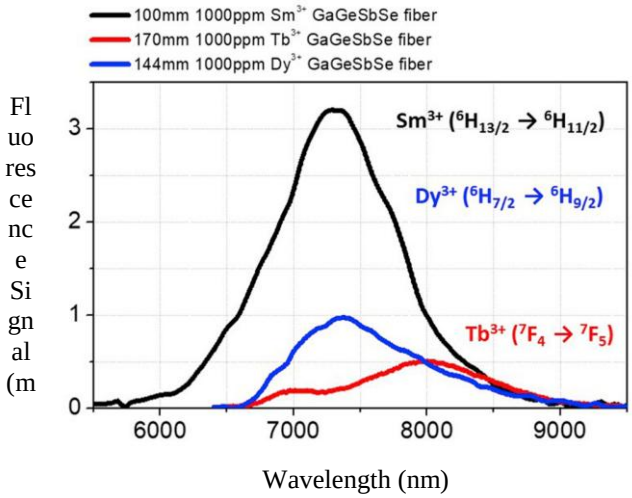

Figure 6 : Luminescence spectra in the 6-9 µm spectral domain from Sm^{3+}, Dy^{3+}, and Tb^{3+} -doped selenide glass fibers [44].

To complete the rare earth series, one should mention Yb^{3+} ions, which have been studied in co-doping configuration for quantum cutting or down-conversion effects in chalco-halide glasses, with the aim to obtain efficient light converters for photovoltaic solar cells based on silicon. Yb^{3+} possesses a unique 4f excited state from which luminescence occurs at around 1µm, through the $^2F_{5/2} \rightarrow {}^2F_{7/2}$ transition. That luminescence is just above the band gap of Si. Thus, quantum cutting is demonstrated in Ce^{3+}/Yb^{3+} codoped chlorosulfide glass with 119 % efficiency [68], while down-conversion takes place in Er^{3+}/Yb^{3+} and Tm^{3+}/Yb^{3+} systems, with quantum efficiency of 114 % in the latter case [69], [70].

4 Chalcogenide-glass optical waveguides doped with rare-earth ions

4.1 Optical fibers

Fibers are essential optical components for applications where light must be transported (power delivery, remote sensing) or confined (high non-linearity). Several types of architecture have been investigated from single-index fibers to single-mode core-clad fibers, not to mention photonic crystal fibers (PCF) with their extreme versatility in terms of cross-

section design. Thanks to an appropriate viscosity-temperature behavior, several chalcogenide glasses can be obtained in the form of wires and fibers by heating a preform in a drawing tower, described elsewhere [71].

Single-index preforms, or rods, are usually prepared by a classical melting-quenching procedure. Core-clad preforms can be elaborated by various methods. The rod-in-tube technique necessitates, in a preliminary step, to elaborate separately a glass rod (core glass) and a glass tube (cladding glass). The two pieces are then inserted one in another, forming the preform. A second method is the double-crucible technique where the preform is obtained directly from the two glass melts. The core and clad diameters are controlled by varying the pressure above the melts [72]. An alternative is the core-on-clad method that utilizes a single crucible, as proposed recently [73]. Chalcogenide photonic crystal fibers or microstructured optical fibers (MOF) are drawn from specific preforms obtained by either the stack-and-draw process [74], or the direct molding process [75], or the drilling process [76], [77]. Optical losses lower than 0.5 dB/m have been measured for As_2Se_3 MOFs prepared by the second method. Chalcogenide glass preforms can also be elaborated by extrusion techniques [78], [79].

When doped with rare-earth ions, optical fibers offer better conditions than bulk glasses to generate light and ultimately obtain light amplification and lasing. This is the case for light emission beyond 6 µm in selenide glasses that requires optical fiber configuration, as shown in the previous paragraph. In the near infrared, one of the best achievement is the demonstration of optical amplification in a Ga-Na-S glass fiber doped with Pr^{3+} ions, reaching a high net gain of 32 dB obtained with pump power of 90 mW at 1.02 µm [60].

Pr^{3+} ions have been extensively studied in selenide-based optical fibers as potential laser sources at wavelengths greater than 4 µm. For that purpose, fibers with small core and low optical losses are required. Thus, step-index fibers with Ge-As-Ga-Se/S glass containing 500 ppmw Pr^{3+} were manufactured with core diameter as small as 10 µm and optical losses as low as 2 dB/m in the 6.5-7.1 µm wavelength region [67]. Broad emission was recorded from 3.5 to 6 µm with pump power of 50.2 mW at 1.55 µm. The experimental lifetime was found to be equal to 7.8 ms. The same value was reported for parent bulk glass, indicating that the numerous steps implemented in the bulk to small-core fiber processing do not affect the photoluminescence decay. In the same glass system, optical losses lower than 1 dB/m were established for small-core fibers thanks to novel multistage techniques of glass purification. These techniques include the use of gallium iodide for vapor phase transport [80]. Enrichment of the germanium content in glass composition lead to a material with a higher glass transition temperature and, hence, with improved ability to withstand strong light flows. Thus, intense luminescence at 4.7 µm could be measured out of a Ge-enriched core-clad selenide fiber doped with Pr^{3+} ions, with an input pump power up to 1.6 W at 1.56 µm [81].
Broad spectral emission in the mid-infrared is of high interest for light sources in sensing applications, in biochemistry, medicine, and environment monitoring, for instance. Thus, milliwatt-level ultra-broad spontaneous emission was measured across the 3.5-8 µm spectral range from a Pr^{3+}-doped selenide multimode fiber pumped with a laser diode at 1.47 µm [82]. The emission spectrum is a combination of at least three transitons: $^3H_6$, $^3F_2 \rightarrow {}^3H_5$, $^3H_5 \rightarrow {}^3H_4$, and $^3F_3 \rightarrow {}^3F_2$. Milliwatt output power was obtained at the end of a 70-mm-long fiber, with nearly 1200 mW pump power. Co-doping is another way to obtain broad spectral emission. Thus, association of Pr^{3+} and Dy^{3+} in the same fiber gives rise to a broad emission in the 2.2-5.5 µm wavelength region, as shown in Figure 7 [83]. A similar study was conducted with co-doped selenide glass fibers, with dual pumping at 1.511 µm and 1.32 µm [84].

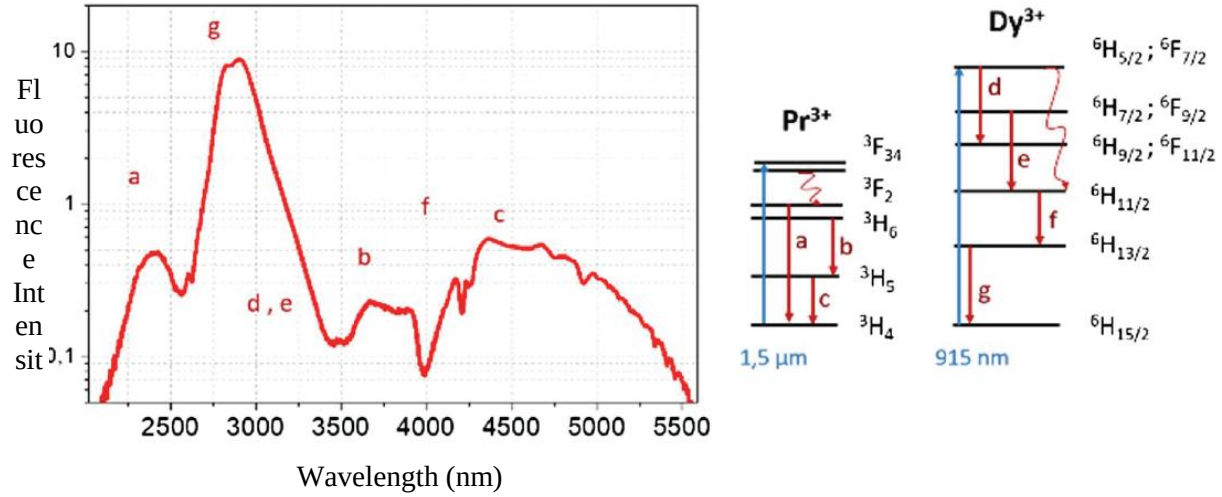

Figure 7 : Broadband emission spectrum from co-doped 1000 ppmw Pr^{3+} / 200 ppmw Dy^{3+} sulfide fiber recorded on a logarithmic scale. Pumping schemes and emission lines contributing to the quasi-continuous spectrum are shown in the energy level diagrams [83].

Optical amplification at wavelength around 4.5 µm was predicted in a Pr^{3+} -doped selenide fiber pumped at 2 µm [85]. The calculation showed that a maximum gain of 16 dB could be achieved with an input signal power of 100 mW. The amplifier gain is expected to be more than 10 dB between 4.25 and 4.55 µm. Gain as high as 25 dB is predicted with input signal power of 10 mW. Experimentally, a maximum gain of 4.6 dB was achieved in a Pr^{3+} -doped selenide fiber resonantly pumped at 4.1 µm [86]. Maximum gains, shown in Figure 8, were obtained at 5.28 and 5.41 µm with 80 mW pump power injected in a 109-mm long fiber. With Dy^{3+}-doped sulfide fibers, modelization demonstrated that, in MOPA (Master Oscillator Power Amplifier) configuration, output power of 637 mW could be achieved at 4.384 µm, with 3-W pump power at 1.709 µm [87]

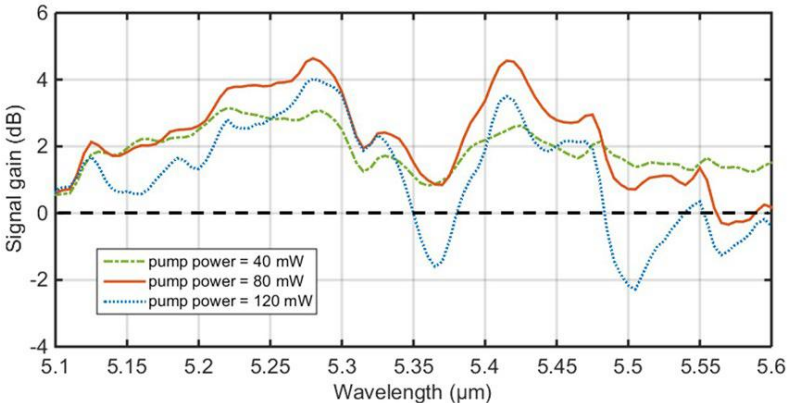

Figure 8 : Signal gain spectrum at pump powers of 40, 80 and 120 mW, respectively, in a 4.1-µm resonantly-pumped Pr^{3+}-doped selenide fiber amplifier [86].

In very recent studies, lasing was demonstrated at wavelengths beyond 5 µm by means of rare-earth-doped selenide-glass step-index fibers. Thus, laser action was obtained for the first time with Tb^{3+} ions at 5.38 µm in a high-purity, small-core (18-µm diameter) fiber pumped at 1.98 µm [88]. Lasing was also achieved at 5.14, 5.17, and 5.28 µm in a Ce^{3+}-doped selenide

glass step-index fiber with a 9-µm core diameter [89]. The 64-mm long fiber was pumped to the $^2F_{7/2}$ excited level of Ce^{3+} with a quantum cascade laser at 4.15 µm. Lasing threshold is at 86-mW pump power.

Rare-earth-doped chalcogenide fibers have been extensively studied as compact infrared light sources for remote sensing of molecules, as introduced in §.3.2. Especially, sensing CO_2 molecules is of high interest in the context of global warming. For this purpose, a device has been developed for monitoring the injection and storage of CO_2 in underground geological sites. Dy^{3+}-doped sulfide glass fibers provide good emission efficiency in the 4 - 4.6 wavelength region, corresponding to the $^6H_{11/2} \rightarrow {}^6H_{13/2}$ transition, with possible excitation in the near infrared at 920 nm. This emission overlaps totally the absorption band of CO_2 molecules around 4.3 µm, as shown in Figure 4. Thus, shining light from a Dy^{3+}-doped sulfide fiber into a cell containing a mixture of CO_2 and N_2 gases allows measurement of the CO_2 concentration by comparing light intensity at the output of the cell, with and without CO_2 molecules [90]. At the laboratory scale, a low detection threshold of 50 ppm CO_2 was achieved with a cell as short as 4 mm in length. This is well below the atmospheric concentration of 400 ppm requested for the targeted application. Then, an experimental set-up, shown in Figure 9 was developed to allow measurement of CO_2, on-site at a depth of 90 m. In that configuration, the excitation light at 920 nm from a laser diode was transported through a silica optical fiber down to 90 m, and, then, injected into a 20-cm long Dy^{3+}-doped sulfide fiber that shines the gas cell. The output signal around 4.4 µm was collected by a non-doped sulfide fiber prior to be detected by a pyroelectric detector. The influence of Dy^{3+} concentration, fiber length, propagation losses and fiber diameter on the 4.4-µm fluorescence has been investigated [91].

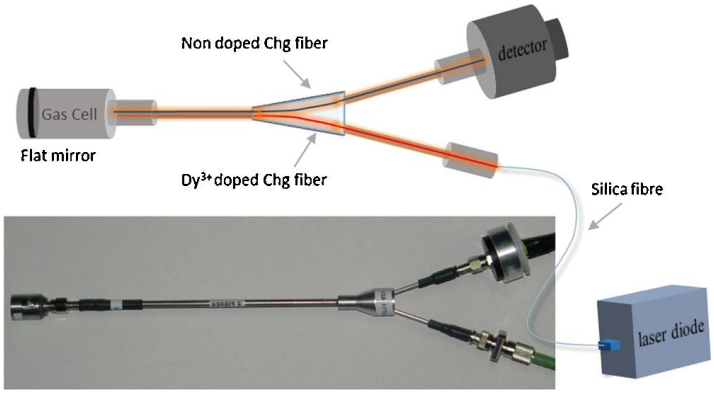

Figure 9 : CO_2 optical sensor head utilizing a Dy^{3+}-doped sulfide fiber emitting around 4.4 µm [46].

The presence of electronic parts in the sensor head described above is a drawback for viable on-site application. Then, an all-optical CO_2 remote sensor was developed, based on the conversion of the 4.4 µm signal at the output of the sensor into light that can be transmitted by silica fibers. The conversion consists in pumping an Er^{3+}-doped sulfide glass fiber with 982-nm light from a laser diode and simultaneously with a 4.4-µm infrared signal [92]. This pump-probe mechanism, described in Figure 10, results in the emission of light at 810 nm from the $^4F_{9/2}$ excited state of Er^{3+} ions, only when the 4.4 µm signal is present. This all-optical sensor was successfully tested on site down to a depth of 80 m [93]. Intrinsically, because of the use of silica fibers to transport light to and from the sensor head, kilometer-range measurements are possible.

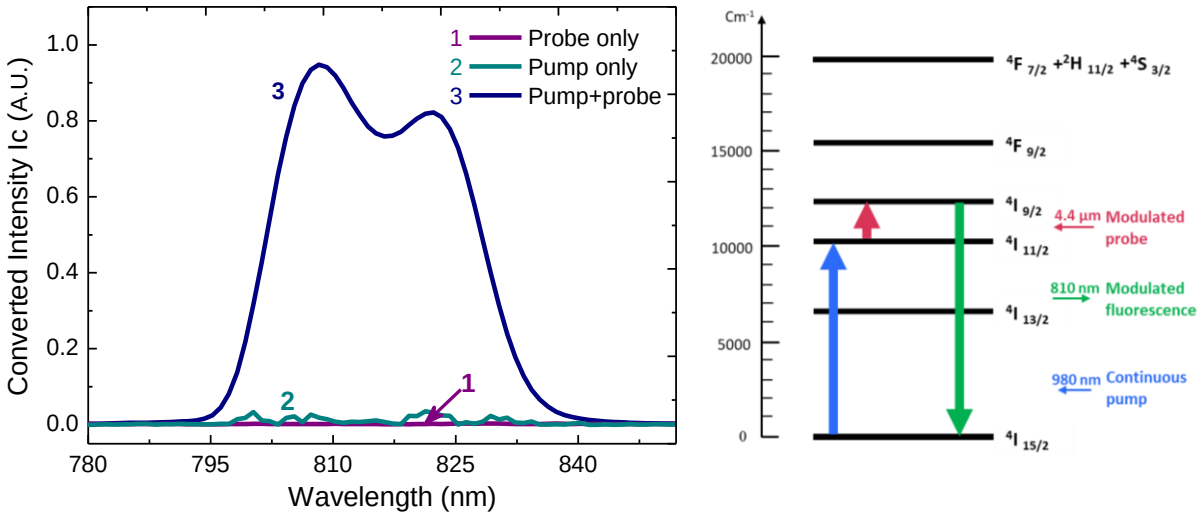

Figure 10 : Emission spectra recorded around 810 nm with a 10^4-ppm Er^{3+} doped Ga-Ge-Sb-S sample under different pumping conditions. 1-modulated IR probe at 4.4 µm, 2-CW pump at 982 nm only and 3-CW pump and modulated probe simultaneous excitation. [92]

4.2 Chalcogenide thin films for integrated photonic circuit

In addition to optical fibers, the fabrication of luminescent optical compounds in integrated optics is essential in modern telecommunication or optical sensing technologies. These optical components can be used to compensate for optical, coupling and splitting losses, as well as to fabricate integrated laser sources, operating in the visible for RGB (red, green and blue), telecommunication or mid-IR bands. Due to the remarkable properties of chalcogenide glasses, thin films are expected to play a leading role in the development of active planar optics integrated circuits for the mid-infrared. Building on mature technologies in the microelectronics industry, silicon-on-insulator (SOI) has emerged over the past two decades as the preferred substrate platform for near-infrared (1.3-1.6 µm) photonic integration, especially for telecom/datacom applications. However, because SiO_2 absorbs strongly for wavelengths longer than 4 µm, other approaches are needed to extend the operating wavelength range of the SOI platform into the mid-IR. Furthermore, due to the indirect band gap of Si and despite recent achievements, the integration of light sources on silicon remains challenging, especially in the mid-IR. Several avenues have opened up for the integration of light sources on Si substrate [94]. They include nonlinear frequency generation or conversion [95], [96] or coupling external III-V semiconductor lasers to Si photonic chips via photonic wire bonds [97]. On-chip integration of III-V lasers can be achieved either through a fully monolithic approach (hetero-epitaxy) or through a combined hybrid-monolithic approach (heterogeneous integration). These integration schemes have been implemented in the telecom [98] and mid-IR wavelength regions [99]. Another option for implementing on-chip lasers on Si photonics could be based on the use of luminescent materials such as rare-earth doped materials as a gain medium. Lasing and net gain have been demonstrated using rare earth and Al_2O_3 doped or Yttrium stabilized zirconia films over Si or silicon nitride waveguides. Near-infrared emission up to ~2 µm has been achieved using Er^{3+} and Tm^{3+} or Ho^{3+} doping, respectively [100], [101], [102], [103]. To extend photonics into the mid-infrared and mitigate

the problem of SiO_2 absorption above 3.6 µm, silicon-integrated chalcogenide waveguides are particularly attractive because they can exhibit mid-infrared transparency and near- and mid-infrared light emission when doped with rare earth ions

Several methods have been proposed for the fabrication of amorphous chalcogenide thin films including CVD techniques, i.e. Chemical Vapor Deposition and PVD, Physical Vapor Deposition techniques and sol-gel soft chemistry [104], [105]. More specifically, the incorporation of rare earths into chalcogenide matrices requires PVD deposition techniques that are either direct or require a subsequent doping step: RF sputtering, PLD, thermal co-evaporation and thermal evaporation with ion implantation. Table 4 describes results from the literature concerning rare-earth doped chalcogenide films and waveguides, including matrices, deposition and waveguide fabrication techniques, and involved transitions.

Table 4: Summary of rare earth doped chalcogenide thin films and waveguides exhibiting infrared luminescence and their fabrication techniques

RE^{3+}	Glass composition	Deposition technique	Waveguide fabrication	Transition	Wavelength	Ref
Pr^{3+}	Ga-Ge-S-CsI	PLD	-	$^1G_4 \rightarrow {}^3H_5$	1.34 µm	[106], [107], [108], [109]
	Ga-Ge-Se	PLD	-	$^1G_4 \rightarrow {}^3H_5$ $^3F_3 \rightarrow {}^3H_4$	1.34 µm 1.6 µm	[110]
	Ga-Ge-Sb-Se	Sputtering	ICP-RIE CHF_3	$(^3H_6, ^3F_2) \rightarrow {}^3H_5$ $^3H_5 \rightarrow {}^3H_4$	3.5-5.5 µm	[111], [112]
Nd^{3+}	As-S	Co-evaporation	-	$^4F_{3/2} \rightarrow {}^4I_{9/2}$ $^4F_{3/2} \rightarrow {}^4I_{11/2}$	0.9 µm 1.1 µm	[113]
Dy^{3+}	Ga-Ge-Sb-S	PLD	-	$(^6H_{9/2} + {}^6F_{11/2}) \rightarrow {}^6H_{15/2}$	1.3 µm	[114]
	Ga-Ge-S-CdI_2 Co-doping Tm^{3+}					[115]
Er^{3+}	Ga-Ge-S	PLD	-	$^4H_{11/2} \rightarrow {}^4I_{15/2}$ $^4S_{3/2} \rightarrow {}^4I_{15/2}$	0.535 µm 0.555 µm	[116]
		Evaporation + Ion implantation	-	$^4I_{13/2} \rightarrow {}^4I_{15/2}$	1.55 µm	[117], [118]
		Bulk glass	Laser writing			[119]
	Ga-Ge-Se	Co-evaporation	-			[120], [121]
		Sputtering	-			[122]
	Ge-As-Se	Evaporation + Ion implantation	-			[123]
	As-S	Co-evaporation	ICP-RIE CHF_3			[124]
		Sputtering RF magnetron	-			[125]
		Evaporation + Ion implantation	Wet etching			[126]
		Co-evaporation	-			[113]
	As-Se	Co-evaporation	-			[113]
		Sputtering RF magnetron	-			[125]
	As-S-Se	Evaporation + Ion implantation	-			[126]
	Ga-La-S	Sputtering	« Lift-off »			[127]
				$^4I_{11/2} \rightarrow {}^4I_{13/2}$	2.7 µm	[128]
	Ga-Ge-(As)-Se	PLD	-	$^4I_{13/2} \rightarrow {}^4I_{15/2}$	1.55 µm	[129]
	Ga-Ge-Sb-	PLD	ICP-RIE			[130]

	S(Se)		CF_4			
	Ga-Ge-Sb-S	Sputtering RF magnetron	ICP-RIE CF_4	$^4I_{11/2}\rightarrow{}^4I_{13/2}$ $^4I_{13/2}\rightarrow{}^4I_{15/2}$	2.8 µm 1.55 µm	[61]
	Ge-As-S-Se	Sputtering	-	$^4I_{13/2}\rightarrow{}^4I_{15/2}$	1.55 µm	[131]
Tm^{3+}	Ga-Ge-S-CdI_2 Co-doping Dy^{3+}	PLD	-	$^3H_5\rightarrow{}^3H_6$ $^3H_4\rightarrow{}^3F_4$ $^3F_4\rightarrow{}^3H_6$	1.22 µm 1.45 µm 1.83 µm	[115]
	Ga-Ge-Sb-S	Sputtering	-	$^3H_5\rightarrow{}^3H_6$ $^3H_4\rightarrow{}^3F_4$	1.25 µm 1.47 µm	[58]

Thermal evaporation is, from a technological point of view, certainly the simplest deposition technique. The main drawback is the difference in evaporation rate between the rare earth ions and the different elements of chalcogenide glasses. Thus, to overcome this difficulty, different methods have been used such as co-evaporation, electron beam assisted evaporation or ion implantation after thin film deposition. Co-evaporation consists in evaporating separately but simultaneously each component of the glass with a different evaporation rate to form the thin film of chalcogenides doped with rare earth ions. This technique made possible the fabrication of Nd^{3+} or Er^{3+} doped thin films in As_2S_3 and As_2Se_3 matrices [113]. However, these matrices are not very favorable hosts for rare earth doping. One can also start directly from the raw materials in the form of metals, metalloids and chalcogenes (in oxidation state 0) with one evaporation source for each chemical component, such as Ge, Ga, Se for obtaining a composition like Ga-Ge-Se:Er^{3+} [121]. However, Ga is difficult to evaporate due to its high melting temperature and low vapor pressure even at high temperature.

After the development of erbium-doped fiber amplifiers, the realization of Er^{3+}-doped waveguides has been widely studied with the aim of fabricating an amplifier on a chip for integration into miniature optical systems [61], [120]. In addition, the ability to have both high gain and unique nonlinear optical performance for the same thin-film deposited material could lead to efficient all-optical signal processing devices with low pump power. The challenge for devices based on erbium-doped thin films is that rare earth ions tend to form clusters when doped to concentration levels required to be operational as planar amplifiers or optical loss compensators, i.e., 10^{20}-10^{21} ions/cm^3 [120]. As a result, the emission efficiency is often significantly reduced and optimization of the choice of host matrix and deposition methods is essential.

In this context, ion implantation has become a practical way to incorporate Er^{3+} ions into thin films made of different optical materials (SiO_2, Al_2O_3, $LiNbO_3$, etc.). The Er^{3+} concentration depth profile can be tailored by varying the energy and fluence of the ions [132]. Using this doping technique Er^{3+} photoluminescence could be observed at 1.55 µm ($^4I_{13/2}\rightarrow{}^4I_{15/2}$) in chalcogenide thin films. The measured lifetime of the $^4I_{13/2}$ excited level was found to be between 1.6 and 2.3 ms. Annealing after implantation tends to increase the lifetime by possible migration of Er^{3+} into active sites [126]. Ion implantation of Er^{3+} has also been performed in electron gun evaporated Ga-Ge-S thin films. In this case, annealing led to a 50% increase in PL at 1540 nm without changing the shape of the emission band [117], [118].

Historically, pulsed laser ablation has been used to maintain the stoichiometry between the thin film and the target, especially for complex materials such as YBaCuO. This technique allows to get rid of the strong difference in vapor tension of the different elements during the

deposition. For example, Ga-Ge-Se thin films have been fabricated and when doped up to 1% with Er^{3+}; they emit at 1.55 µm [129].

Unlike thermal evaporation, sputtering is a non-thermal deposition process that allows the deposition of elements with different vapor pressures such as rare earths and chalcogenides. Despite this advantage, sputtering of rare-earth doped chalcogenide glasses has not been studied much. The first result consists in the sputtering of a target fabricated by "hot-pressing" of crushed glass $Ge_{10}As_{40}S_{25}Se_{25}$ and powdered Er_2S_3. Photoluminescence of Er^{3+} was observed at 1550 nm in a planar guide and a channel guide made by laser irradiation [131].

It should be noted that relatively few publications mention results on samples with channeled guides allowing at the same time a relatively efficient fluorescence in propagative mode, limited optical losses and a concentration of erbium ions high enough to be adapted to integrated optics. They are all the more rare when it comes to demonstrating luminescence in the mid-infrared. In the most accomplished studies with Ga-La-S:Er^{3+}, (sputtering, [127], [133]), As_2S_3:Er^{3+} (co-evaporation, [62]), Ga-Ge-Sb-S:Er^{3+} (sputtering, [61]), and Ga-Ge-Se:Er^{3+} (co-evaporation, [120]), it was attempted to obtain amplification at 1.5 µm and even luminescence at 2.7 µm on waveguides fabricated by the lift-off photolithographic method or by reactive ion etching (RIE), as shown in Figure 11.

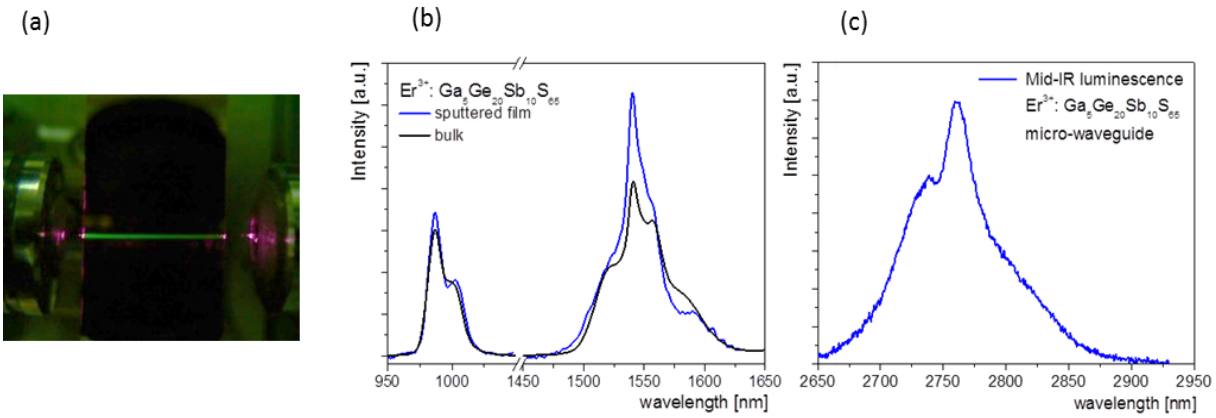

Figure 11 : Image of up-conversion green luminescence along the waveguide optical path (a), comparison of Er^{3+}-$Ga_5Ge_{20}Sb_{10}S_{65}$ emission spectra between the sputtered layer and the corresponding bulk glass (b), guided fluorescence at 2.76 µm from an Er^{3+}-$Ga_5Ge_{20}Sb_{10}S_{65}$-based waveguide [61]

Erbium-doped GaLaS has been used to make ribbon waveguides by photolithography and "lift-off" for amplification purposes. The potential of GaLaS as a laser material was demonstrated in a bulk Nd^{3+} doped glass where channeled guides were photoinduced by UV irradiation with optical losses below 0.5 $dB.cm^{-1}$; however, the integration of the system remained very challenging [134]. The Er^{3+}:GaLaS sputtered waveguides showed an internal gain of 2.8 $dB.cm^{-1}$ with a pump at 1480 nm and a signal at 1550 nm. The optical losses were estimated to be 2.4 ± 0.4 $dB.cm^{-1}$ and are therefore counterbalanced by the internal gain. Moreover, additional optical losses must be taken into account such as the absorption of erbium at this wavelength, of the order of 5.4 $dB.cm^{-1}$ [127]. With the same process, including

an additional step of substrate annealing at 525 °C, the emission at 2.7 µm ($^4I_{11/2} \rightarrow {}^4I_{13/2}$) of Er^{3+} was obtained [128]. More recently, Er^{3+}-doped Ga-Ge-Se films and waveguides have been deposited by thermal co-evaporation and fabricated by plasma etching, as shown in Figure 12, in order to obtain an amplification at telecom wavelengths [120], [121].

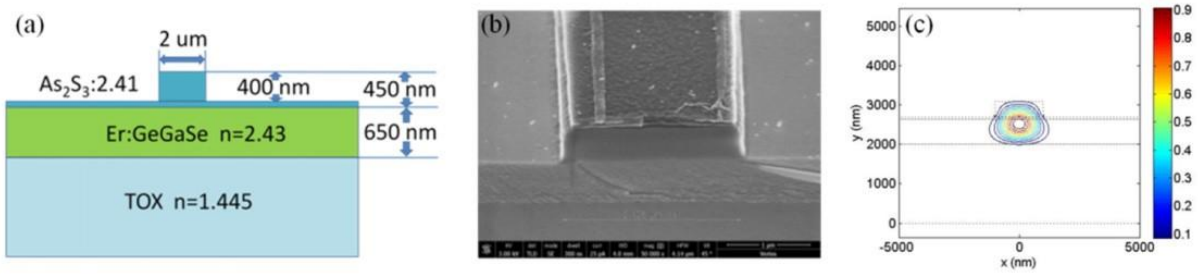

Figure 12: (a) Schematic of the designed structure, (b) cross section of the 2 µm waveguide obtained by SEM and (c) simulated TE fundamental mode for the 2-µm waveguide [120].

For the fabrication of Er^{3+} doped thin films by RF magnetron sputtering, the targets used were massive glasses belonging to the Ga-Ge-Sb-S system [135]. For a good solubility of rare earth ions in the host matrix, gallium was incorporated in the Ge-Sb-S system in order to obtain rare earth ion doped films. Taking into account the length of the waveguide, a gain of 3.4 $dB.cm^{-1}$ on/off was achieved at 1.54 µm. This value is higher than the gains of 2.5 and 2.8 $dB.cm^{-1}$ on/off reported by Sabapathy et al. for an ultrafast laser written Er^{3+}-doped GeGaS glass buried waveguide amplifier [119] and Frantz et al. for Er^{3+}:GaLaS sputtered waveguide [127], respectively. Subtracting the contribution of Er^{3+} absorption, the internal gain is -0.3 $dB.cm^{-1}$, although slightly negative it is also higher than the gain observed at the same wavelength below -4.5 $dB.cm^{-1}$ in Er-doped As_2S_3 chalcogenide waveguide [124].

The integration of multiple monolithic components on a single substrate is beneficial for minimizing size and cost by enabling system-on-chip applications. The demonstration of monolithic light sources emitting in different wavelength regimes is a key component of these systems. Several designs of micro-sphere, micro-disk, optical micro-resonator or multimode multiplexed interferometer (MMI) have been proposed based on rare earth doped chalcogenide films [136], [137], [138], [139]. They are detailed in Figure 13.

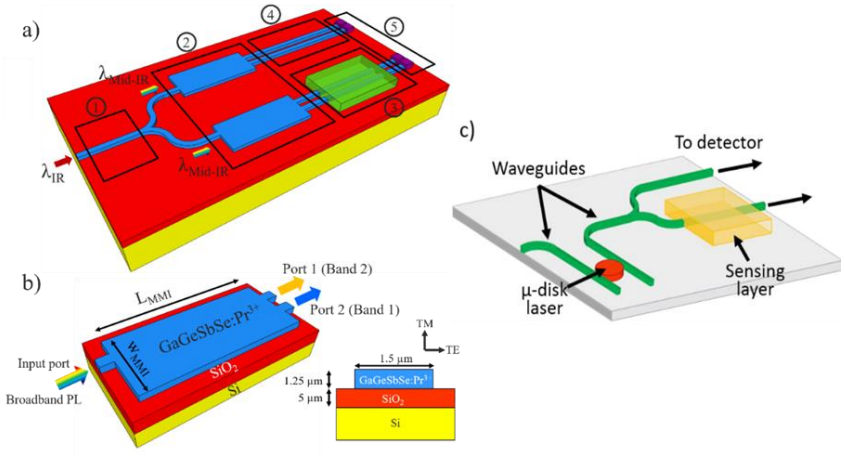

Figure 13: Schematic diagram of two types of proposed sensing platform based on a multimode multiplexed interferometer (MMI) (a and b) or a GaGeSbSe:Pr^{3+} based microdisk lases (c), evanescent transducer and microfluidic cell, reference arms and sensing stage [139].

The conception and fabrication of these components are under progress for Ge-based sputtered thin films emitting in mid-IR [111], [112], [138], [139]. Some components have already been achieved, as shown in Figure 14. The main technological hurdles to overcome concern: i) the optimization of rare earth ion doped materials to achieve efficient fluorescence, ii) the determination and minimization of the phenomena responsible for the intrinsic optical losses to obtain a high gain, iii) the reduction of the surface roughness of the component for a consistent quality factor ($Q>10^6$).

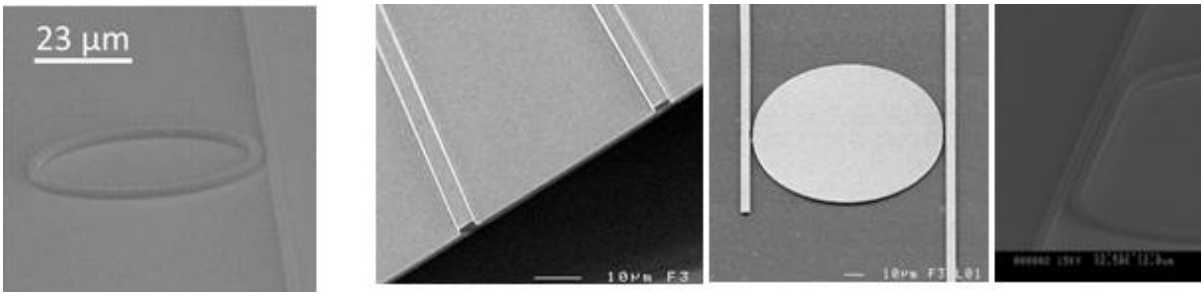

Figure 14: Chalcogenide optical waveguides, microdisks and micro-resonators obtained by reactive physical etching of Ge-based sputtered thin films.

Praseodymium-doped Ga-Ge-Sb-Se co-pulverized waveguides have been shown to be operating materials for infrared signal generation and propagation, and are therefore promising devices in the NWIR and MWIR fields. By comparing waveguides with various concentrations of praseodymium, the optimal doping for maximum fluorescence intensity was identified to be near 4100 ppm, where the most intense emission was recorded at both 2.5 and 4.5 µm wavelengths. Spectra recorded in the 4.5 µm region for different optical excitation densities at 1.55 µm (waveguide width = 10 µm) are shown in Figure 15.

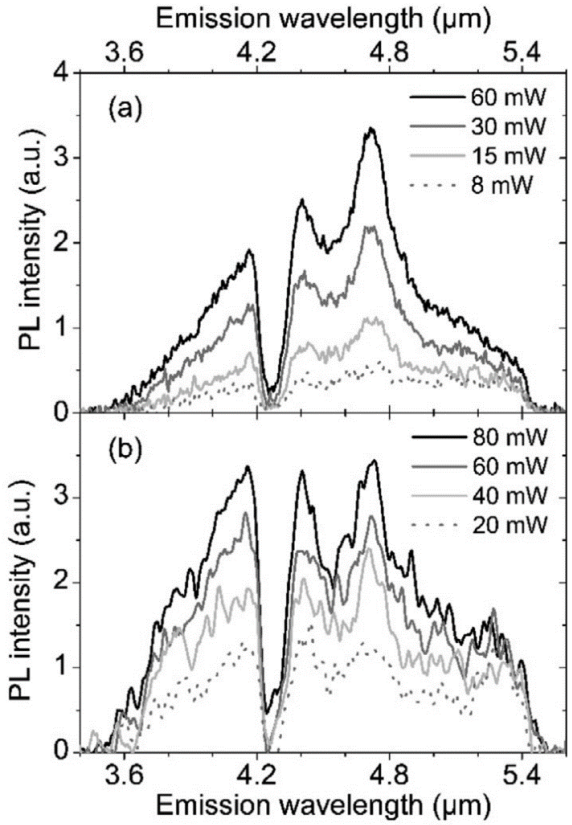

Figure 15: GaGeSbSe:Pr^{3+} waveguide photoluminescence on SiO_2 (a) and $Ge_{28}Sb_6Se_{66}$ (b) thin film [111].

Conclusion

In conclusion, the paper reviewed the unique optical properties of chalcogenide glasses, especially in terms of rare-earth luminescence in the infrared domain. Luminescence is reported at wavelengths ranging from the near- to mid-infrared, offering a quasi-continuum of infrared light sources. The most significant results are summarized below.

Laser action was obtained at 1 μm in bulk and channel waveguide configurations with Nd^{3+}-doped Ga-La-S glass. With Pr^{3+}, optical amplification was demonstrated in a Ga-Na-S glass fiber. A high net gain of 32 dB was obtained with pump power of 90 mW at 1.02 μm.

On/off gains and internal gains were measured at 1.54 μm in Er^{3+}-doped planar and channel waveguides made of different glasses ($Ge_{20}Ga_5Sb_{10}S_{65}$, As_2S_3, GaLaS). Broad luminescence centered at 2.77 μm was measured in Er^{3+}-doped $Ge_{20}Ga_5Sb_{10}S_{65}$ and GaLaS channel waveguides.

Emissions at wavelengths around 3 μm and above were achieved in both sulfide and selenide glasses. These transitions are of interest as sources for optical sensing and for signal transmission in the 3-5 μm transparency window of the atmosphere. The broad 4.4 μm emission of Dy^{3+} was successfully utilized to perform quantitative detection of CO_2 gas. Er^{3+} ions possess also a transition that coincides with CO_2 absorption. That transition is from $^4I_{9/2}$ to $^4I_{11/2}$, spanning the 4.3 - 4.8 μm spectral band. In that same spectral region, the combination of Pr^{3+} transitions at 3.9 and 4.8 μm leads to a super-broad band spanning from 3.5 to 5.5 μm in bulk glass and single-index fiber. Besides, a maximum gain of 4.6 dB was achieved in a 109-mm-long, Pr^{3+}-doped, selenide fiber resonantly pumped at 4.1 μm. Mid-infrared guided

photoluminescence from integrated Pr^{3+}-doped selenide ridge waveguides was obtained in the range of 3.5-5µm.

In very recent studies, lasing was demonstrated at wavelengths beyond 5 µm by means of rare-earth-doped selenide-glass step-index fibers. Thus, laser action was obtained for the first time with Tb^{3+} ions at 5.38 µm in a high-purity small-core fiber. Lasing was also achieved at 5.14, 5.17, and 5.28 µm in a 64-mm-long, Ce^{3+}-doped, selenide glass step-index fiber with a 9-µm core diameter.

Luminescence was observed at wavelengths greater than 6 µm in rare-earth-doped selenide glass fibers doped with Sm^{3+}, Tb^{3+}, and Dy^{3+}. The most intense emission is obtained at 7.2 µm with a 100-mm long fiber doped with 1000 ppm Sm^{3+}

References

[1] X.-H. Zhang, J.-L. Adam, B. Bureau, Chalcogenide glasses, in J.D. Musgraves, J. Hu, L. Calvez (Eds), Handbook of Glass, Springer, 2019, pp 525-552

[2] B.G. Aitken, C.W. Ponader, R.S. Quimby, Clustering of rare earths in GeAs sulfide glass. Comptes Rendus Chimie 5 (2002) 865-872

[3] Y. Guimond, J.-L. Adam, A.M. Jurdyc, H.-L. Ma, J. Mugnier, B. Jacquier, Optical properties of antimony-stabilized sulfide glasses doped with Dy^{3+} and Er^{3+} ions, J. Non-Cryst. Solids 256&257 (1999) 378-82

[4] J. Troles , Y. Niu, C. Duverger-Arfuso, F. Smektala, L. Brilland, V. Nazabal, V. Moizan, F. Desevedavy, P. Houizot, Synthesis and characterization of chalcogenide glasses from the system Ga–Ge–Sb–S and preparation of a single-mode fiber at 1.55 µm, Mater. Res. Bull. 43 (2008) 976–982

[5] R. Chahal, F. Starecki, J.L. Doulan, P. Nemec, A. Trapananti, C. Prestipino, G. Tricot, C. Boussard-Plédel, K. Michel, A. Braud, P. Camy, J.L. Adam, B. Bureau, V. Nazabal, Nd^{3+} : Ga-Ge-Sb-S glasses and fibers for luminescence in mid-IR : synthesis, structural characterization and rare-earth spectroscopy, Opt. Mater. Expr. 8 (2018) 1650

[6] A. Ravagli, M. Naftaly, C. Craig, E. Weatherby, D.W. Hewak, Dielectric and structural characterisation of chalcogenide glasses via terahertz time-domain spectroscopy, Opt. Mater. 69 (2017) 339-343

[7] A. Ravagli, C. Craig, J. Lincoln, D. W. Hewak, Ga-La-S-Se glass for visible and thermal imaging, Adv. Opt. Techn. 6 (2017) 131–136

[8] Amorphous Materials Inc., USA, AMTIR-6 Datasheet http://www.amorphousmaterials.com/products/

[9] H.L. Ma, Y. Guimond, X.H. Zhang, J. Lucas, Ga–Ge–Sb–Se based glasses and influence of alkaline halide addition, J. Non-Cryst. Solids 256-257 (1999) 165-169

[10] Refractive Index Data Base https://refractiveindex.info/?shelf=glass&book=AMTIR&page=AMTIR-1

[11] A. Zakery, S.R. Elliot, Optical nonlinearities in chalcogenide glasses and their applications in: Springer Series in Optical Sciences, Vol. 135, Springer, Berlin, 2007

[12] J.A. Savage, S. Nielsen, Chalcogenide glasses transmitting in the infrared between 1 and 20 µm - A state of the art review, Infrared Phys. 5 (1965) 195-204

[13] C. Gonçalves, R. Mereau, V. Nazabal, C. Boussard-Plédel, C. Roiland, E. Furet, M. Deschamps, B. Bureau, M. Dussauze, Study of the $Ge_{20}Te_{80-x}Se_x$ glassy structures by

combining solid state NMR, vibrational spectroscopies and DFT modelling, J. Solid State Chem. 297 (2021) 122062
[14] N. Abdellaoui, F. Starecki, C. Boussard-Plédel, Y. Shpotyuk, J.L. Doualan, A. Braud, E. Baudet, P. Nemec, F. Cheviré, M. Dussauze, B. Bureau, P. Camy, V. Nazabal, Tb^{3+} doped $Ga_5Ge_{20}Sb_{10}Se_{65-x}Te_x$ (x=0-37.5) chalcogenide glasses and fibers for MWIR and LWIR emissions, Opt. Mater. Expr. 8 (2018) 2887-2900
[15] G. Delaizir, M. Dussauze, V. Nazabal, P. Lecante, M. Dollé, P. Rozier, E.I. Kamitsos, P. Jovari, B. Bureau, Structural characterizations of As–Se–Te glasses, J. Alloys Comp. 509 (2011), 831-836
[16] L. Calvez, H.L. Ma, J. Lucas, X.H. Zhang, Selenium-based glasses and glass ceramics transmitting light from the visible to the far-IR, Adv. Mater. 19 (2007) 129-132
[17] V.S. Shiryaev, M.F. Churbanov, Preparation of high-purity chalcogenide glasses, in: J.L. Adam, X.H. Zhang (Eds), Chalcogenide glasses, preparation, properties and applications, Woodhead Pub. Ltd, Cambridge, 2014, pp. 3-35
[18] A.P. Velmuzhov, M.V. Sukhanov, N.S. Zernova, V.S. Shiryaev, T.V. Kotereva, L.A. Ketkova, I.I. Evdokimov, A.E. Kurganova, Preparation of $Ge_{20}Se_{80}$ glasses with low hydrogen and oxygen impurities content for middle IR fiber optics, J. Non-Cryst. Solids 521 (2019) 119505
[19] H. Guo, J. Cui, C. Xu, Y. Xu, G. Farrell, Mid-infrared spectral properties of rare earth ion doped chalcogenide glasses and fibers, in J. Atai, R. Liang, U. S. Dinish (Eds), Mid-infrared fluoride and chalcogenide glasses and fibers, Progress in Optical Science and Photonics, Volume 18, Springer, 2022, pp 217-283
[20] C. B. Layne, W. H. Lowdermilk, M. J. Weber, Multiphonon relaxation of rare-earth ions in oxide glasses, Phys. Rev. B 16 (1977) 10-20
[21] M.D. Shinn, W.A. Sibley, M.G. Drexhage, R.N. Brown, Optical transitions of Er^{3+} ions in fluorozirconate glass, Phys. Rev. B 27 (1983) 6635-6648
[22] J.L. Adam, W.A. Sibley, Optical transitions of Pr^{3+} ions in fluorozirconate glass, J. Non-Cryst. Solids 76 (1985) 267-279
[23] J.L. Adam, M. Matecki, J. Lucas, Multiphonon relaxations in chloro-fluoride glasses, J. Non-Cryst. Solids 184 (1995) 119-123
[24] V.G. Truong, B.S. Ham, A.M. Jurdyc, B. Jacquier, J. Le Person, V. Nazabal, J.L. Adam, Relaxation properties of rare-earth ions in sulfide glasses: experiment and theory, Phys. Rev. B 74, 184103 (2006)
[25] R.S. Quimby, B.G. Aitken, Multiphonon energy gap law in rare-earth doped chalcogenide glass, J. Non-Cryst. Solids 320 (2003) 100-112
[26] R. Reisfeld, Fluorescence and nonradiative relaxations of rare-earths in amorphous media and on high surface area supports: a review, J. Electrochem. Soc. 131 (1984) 1360-1364
[27] Y.B. Shin, W.Y. Cho, J. Heo, Multiphonon and cross relaxation phenomena in Ge-As (or Ga)-S glasses doped with Tm^{3+}, J. Non-Cryst. Solids 208 (1996) 29-35
[28] Y.B. Shin, J. Heo, H.S. Kim, Enhancement of the 1.31-μm emission properties of Dy^{3+}-doped Ge-Ga-S glasses with the addition of alkali halides, J. Mater. Res. 16 (2001) 1318-1324
[29] J. Ren, X. Lu, C. Lin, R.K. Jain, Luminescent ion-doped transparent glass ceramics for mid-infrared light sources, Opt. Express 28 (2020) 21522

[30] M. F. Churbanov, B. I. Denker, B. I. Galagan, V. V. Koltashev, V. G. Plotnichenko, S. M. V. Sukhanov, E. Sverchkov, A. P. Velmuzhov, Cascade sensitization of mid-infrared Ce^{3+} luminescence by Dy^{3+} ions in selenide glass, J. Lumin. 231 (2021) 117809
[31] J.S. Sanghera, I.D. Aggarwal, Active and passive chalcogenide glass optical fibers for IR applications: a review, J. Non-Cryst. Solids 256&257 (1999) 6-16
[32] D. R. Simons, A.J. Faber, H. De Waal, GeSx glass for Pr^{3+}-doped fiber amplifiers at 1.3 μm. J. Non-Cryst. Solids 185 (1995) 283-288
[33] L.B. Shaw, B.B. Harbison, B. Cole, J.S. Sanghera, I.D. Aggarwal, Spectroscopy of the IR transitions in Pr^{3+} doped heavy metal selenide glasses. Optics Express 1 (1997) 87-96
[34] M. F. Churbanov, B. I. Denker, B. I. Galagan, V. V. Koltashev, V. G. Plotnichenko, S. E. Sverchkov, M. V. Sukhanov, A. P. Velmuzhov, Peculiarities of 1.6-7.5 μm Pr^{3+} luminescence in $Ge_{36}Ga_5Se_{59}$ glass, Opt. Mater. Expr. 9 (2019) 4154-64
[35] L.B. Shaw, B. Cole, P.A. Thielen, J.S. Sanghera, I.D. Aggarwal, Mid-wave IR and long-wave IR laser potential of rare-earth doped chalcogenide glass fiber, IEEE J. Quant. Electron. 48 (2001) 1127-1137
[36] H. Sakr, D. Furniss, Z. Tang, L. Sojka, N. A. Moneim, E. Barney, S. Sujecki, T. M. Benson, A. B. Seddon, Superior photoluminescence (PL) of Pr^{3+}-In, compared to Pr^{3+}-Ga, selenide-chalcogenide bulk glasses and PL of optically-clad fiber, Opt. Express 22 (2014) 21236
[37] T. Schweizer, B.N. Samson, R.C. Moore, D.W. Hewak, D.N. Payne, Rare-earth doped chalcogenide glass fiber laser, Electron. Lett. 32 (1996) 666-667
[38] P. Nemec, J. Oswald, M. Frumar, M. Frumarova, Optical properties of germanium-gallium-selenide glasses doped by samarium, J. Optoelectron. Adv. Mater. 1 (1999) 33
[39] F. Starecki, A. Braud, N. Abdellaoui, J.-L. Doualan, C. Boussard-Plédel, B. Bureau, P. Camy, V. Nazabal, 7 to 8 μm emission from Sm^{3+} doped selenide fibers, Opt. Expr. 26 (2018) 26462-9
[40] R.W. Crane, L. Sojka, D. Furniss, J. Nunes, E. Barney, M.C. Farries, T.M. Benson, S. Sujecki, A.B. Seddon, Experimental photoluminescence and lifetimes at wavelengths including beyond 7 microns in Sm^{3+} -doped selenide-chalcogenide glass fibers, Opt. Express 28 (2020) 12373-384
[41] F. Starecki, N. Abdellaoui, A. Braud, J.-L. Doualan, C. Boussard-Plédel, B. Bureau, P. Camy, V. Nazabal, 8 μm luminescence from a Tb^{3+} GaGeSbSe fiber, Opt. Lett. 43 (2018) 1-4
[42] L. Sojka, Z. Tang, H. Sakr, D. Furniss, T.M. Benson, A.B. Seddon, E. Barney, E. Beres-Pawlik, S. Sujecki, Spectroscopy of mid-infrared (4.8μm) photoluminescence in Tb^{3+} doped chalcogenide glass and fibre, 17th International Conference on Transparent Optical Networks (ICTON), 2015, pp. 1-3, doi: 10.1109/ICTON.2015.7193669
[43] T. Schweizer, B.N. Samson, J.R. Hector, W.S. Brocklesby, D.W. Hewak, D.N. Payne, Infrared emission and ion–ion interactions in thulium- and terbium-doped gallium lanthanum sulfide glass, J. Opt. Soc. Amer. B 16 (1999) 308-316
[44] F. Starecki, G. Louvet, J. Ari, A. Braud, J.-L. Doualan, R. Chahal, I. Hafienne, C. Boussard-Plédel, V. Nazabal, P. Camy, Dy^{3+} doped GaGeSbSe fiber long-wave infrared emission, J. Lumin. 218 (2020) 116853
[45] Y. Guimond, J.L. Adam, A.M. Jurdyc, J. Mugnier, B. Jacquier, X.H. Zhang, Dy^{3+}-doped stabilized GeGaS glasses for 1.3 μm optical fiber amplifiers, Opt. Mater. 12 (1999) 467-471

[46] F. Starecki, F. Charpentier, J.-L. Doualan, L. Quetel, K. Michel, R. Chahal, J. Trolès, B. Bureau, A. Braud, P. Camy, V. Moizan, V. Nazabal, Mid-IR optical sensor for CO_2 detection based on fluorescence absorbance of Dy^{3+}:$Ga_5Ge_{20}Sb_{10}S_{65}$ fibers, Sensors Actuat. B 207 (2015) 518-525
[47] M. Zhang, A. Yang, Y. Peng, B. Zhang, H. Ren, W. Guo, Y. Yang, C. Zhai, Y. Wang, Z. Yang, D. Tang, Dy^{3+}-doped Ga-Sb-S chalcogenide glasses for mid-infrared lasers, Mater. Res. Bull. 70 (2015) 55-59
[48] T. Schweizer, D.W. Hewak, B.N. Samson, D.N. Payne, Spectroscopic data of the 1.8-, 2.9-, and 4.3-μm transitions in dysprosium-doped gallium lanthanide sulfide glass, Opt. Lett. 21 (1996) 1594-1596
[49] T. Schweizer, D.W. Hewak, B.N. Samson, D.N. Payne, Spectroscopy of potential mid-infrared laser transitions in gallium lanthanum sulphide glass, J. Lumin. 72-74 (1997) 419-421
[50] A. Yang, M. Sun, H. Ren, H. Lin, X. Feng, Z. Yang, Dy^{3+} -doped Ga_2S_3-Sb_2S_3-La_2S_3 chalcogenide glass for mid-infrared laser medium, L. Lumin. 237 (2021) 118169
[51] M. Sun, A. Yang, H. Ren, S. Qi, H. Lin, X. Feng, Z. Yang, Mid-infrared luminescence of dysprosium-doped gallium-antimony-sulfur-iodine chalcohalide glasses and fibers, J. Non-Cryst. Solids 560 (2021) 120718
[52] J. Heo, Optical characteristics of rare-earth-doped sulphide glasses, J. Mater. Sci. Lett. 14 (1995) 1014-16
[53] Y.B. Shin, J.N. Jang, J. Heo, Mid-Infrared light emission characteristics of Ho^{3+}-doped chalcogenide and heavy-metal oxide glasses, Opt. Quant. Electron. 27 (1995) 379-386
[54] S. Wei, Y. Xu, S. Dai, Y. Zhou, C. Lin, P. Zhang, Theoretical studies on mid-infrared amplification in Ho^{3+}-doped chalcogenide glass fibers, Physica B 416 (2013) 64–68
[55] C.C. Ye, D.H. Hewak, M. Hempstead, B.N. Samson, D.N. Payne, Spectral properties of Er^{3+} -doped gallium lanthanum sulphide glass, J. Non-Cryst. Solids 208 (1996) 56-63
[56] V. Moizan, V. Nazabal, J. Trolès, P. Houizot, J.L. Adam, F. Smektala, J.L. Doualan, R. Moncorgé, G. Canat, Er^{3+}-doped GeGaSbS glasses for mid-IR fiber laser applications: synthesis and rare-earth spectroscopy, Opt. Mater 31 (2008) 39-46
[57] V.G. Truong, B.S. Ham, A.M. Jurdyc, B. Jacquier, J. Le Person, V. Nazabal, J.L. Adam, Relaxation properties of rare-earth ions in sulfide glasses: experiment and theory, Phys. Rev. B 74 (2006) 184103
[58] V. Nazabal, A.-M. Jurdyc, P. Nemec, M.-L. Brandily-Anne, L. Petit, K. Richardson, P. Vinatier, C. Bousquet, T. Cardinal, S. Pechev, J.-L. Adam Amorphous, Tm^{3+}-doped sulphide thin films fabricated by sputtering, Opt. Mater. 33 (2010) 220-226
[59] A. Galstyan, S.H. Messaddeq, V. Fortin, I. Skripachev, R. Vallée, T. Galstian, Y. Messaddeq, Tm^{3+} doped Ga-As-S chalcogenide glasses and fibers, Opt. Mater. 47 (2015) 518-523
[60] H. Tawarayama, E. Ishikawa, K. Yamanaka, K. Itoh, K. Okada, H. Aoki, H. Yanagita, Y. Matsuoka, H. Toratani, Optical amplification at 1.3 μm in a praseodymium-doped sulfide-glass fiber, J. Am. Ceram. Soc. 83 (2000) 792-796
[61] V. Nazabal, F. Starecki, J.L. Doualan, P. Němec, P. Camy, H. Lhermite, L. Bodiou, M.L. Anne, J. Charrier, J.L. Adam, Luminescence at 2.8 μm: Er^{3+}-doped chalcogenide micro-waveguide, Opt. Mater. 58 (2016) 390-397
[62] K. Yan, K. Vu, S. Madden, Internal gain in Er-doped As_2S_3 chalcogenide planar waveguide, Opt. Lett. 40 (2015) 796-799

[63] S. Kasap, K. Koughia, G. Soundararajan, M. G. Brik, Optical and Photoluminescence Properties of Erbium-Doped Chalcogenide Glasses (GeGaS:Er), IEEE J. Selec. Topics Quant. Electron. 14 (2008) 1353-60
[64] F. Charpentier, F. Starecki, J.L. Doualan, P. Jovari, P. Camy, J. Trolès, S. Belin, B. Bureau, V. Nazabal, Mid-IR luminescence of Dy^{3+} and Pr^{3+} doped $Ga_5Ge_{20}Sb_{10}S(Se)_{65}$ bulk glasses and fibers, Mater. Lett. 101 (2013) 21-24
[65] A. Pelé, A. Braud, J.L. Doualan, F. Starecki, V. Nazabal, R. Chahal, C. Boussard-Plédel, B. Bureau, R. Moncorgé, P. Camy, Dy^{3+} doped GeGaSbS fluorescent fiber at 4.4 µm for optical gas sensing: comparison of simulation and experiment, Opt. Mater. 61 (2016) 37-44
[66] R. Chahal, F. Starecki, C. Boussard-Plédel, J.L. Doualan, K. Michel, L. Brilland, A. Braud, P. Camy, B. Bureau, V. Nazabal, Fiber evanescent wave spectroscopy based on IR fluorescent chalcogenide fibers, Sensors Actuat. B 229 (2016) 209-21
[67] Z. Tang, D. Furniss, M. Fay, H. Sakr, L. Sojka, N. Neate, N. Weston, S. Sujecki, T.M. Benson, A.B. Seddon, Mid-infrared photoluminescence in small-core fiber of praseodymium-ion doped selenide bases chalcogenide glass, Opt. Mater. Exp. 5 (2015) 870-886
[68] B. Gao, Q. Yan, X. Zhang, H. Ma, J.L. Adam, J. Ren, G. Chen, Highly efficient near-infrared quantum cutting in Ce^{3+} / Yb^{3+} co-doped chalcohalide glasses, J. Lumin. 143 (2013) 181-184
[69] B. Fan, C. Point, J.L. Adam, X. Zhang, X. Fan, H. Ma, Near-infrared down-conversion in rare-earth-doped chloro-sulfide glass GeS_2-Ga_2S_3-CsCl : Er, Yb, J. Appl. Phys. 110 (2011) 113107
[70] F. Huang, L. Chen, Y. Han, J. Tang, Q. Nie, P. Zhang, Y. Xu, Visible to near-infrared downconversion in Tm^{3+} / Yb^{3+} co-doped chalcohalide glasses for solar spectra converter, Infrared Phys. Technol. 71 (2015)159-162
[71] V.S. Shiryaev, J.-L. Adam, X.H. Zhang, C. Boussard-Plédel, J. Lucas, M. F. Churbanov, Infrared fibers based on Te-As-Se glass system with low optical losses, J. Non-Cryst. Solids 336 (2004) 113-119
[72] W.H. Kim, V.Q. Nguyen, L.B. Shaw, L.E. Busse, C. Florea, D.J. Gibson, R.R. Gattass, S.S. Bayya, F.H. Kung, G.D. Chin, R.E. Miklos, I.D. Aggarwal, J.S. Sanghera, Recent progress in chalcogenide fiber technology at NRL, J. Non. Cryst. Solids 431 (2016) 8-15
[73] H.S. Seo, B.J. Park, H.R. Choi, J.T. Ahn, Core-on-clad method for fabricating mid-infrared optical fibers, J. Non-Cryst. Solids 431 (2016) 72-75
[74] L. Brilland, F. Smektala, G. Renversez, T. Chartier, J. Trolès, T. N. Nguyen, N. Traynor, A. Monteville, Fabrication of complex structures of holey fibers in chalcogenide glass, Opt. Express 14 (2006) 1280-1285
[75] Q. Coulombier, L. Brilland, P. Houizot, T. Chartier, T. N. N'Guyen, F. Smektala, G. Renversez, A. Monteville, D. Méchin, T. Pain, H. Orain, J. C. Sangleboeuf, J. Trolès, Casting method for producing low-loss chalcogenide microstructured optical fibers, Opt. Express 18 (2010) 9107-9112
[76] M. El-Amraoui, G. Gadret, J. C. Jules, J. Fatome, C. Fortier, F. Désévédavy, I. Skripatchev, Y. Messaddeq, J. Trolès, L. Brilland, W. Gao, T. Suzuki, Y. Ohishi, and F. Smektala, Microstructured chalcogenide optical fibers from As2S3 glass: towards new IR broadband sources, Opt. Express 18 (2010) 26655-26665

[77] P. Zhang, J. Zhang, P. Yang, S. Dai, X. Wang, W. Zhang, Fabrication of chalcogenide glass photonic crystal fibers with mechanical drilling, Opt. Fiber Technol. 26 (2015) 176-179
[78] Z. Tang, V. S. Shiryaev, D. Furniss, L. Sojka, S. Sujecki, T. M. Benson, A. B. Seddon, M. F. Churbanov, Low loss Ge-As-Se chalcogenide glass fiber, fabricated using extruded preform, for mid-infrared photonics, Opt. Mater. Express 5 (2015) 1722-1737
[79] C. Jiang, X. Wang, M. Zhu, H. Xu, Q. Nie, S. Dai, G. Tao, X. Shen, C. Cheng, Q. Zhu, F. Liao, P. Zhang, P. Zhang, Z. Liu, X.H. Zhang, Preparation of chalcogenide glass fiber using an improved extrusion method, Opt. Engineer. 55 (2016) 056114
[80] V.S. Shiryaev, M.F. Churbanov, Recent advances in preparation of high-purity chalcogenide glasses for mid-IR photonics, J. Non-Cryst. Solids 475 (2017) 1-9
[81] V.S. Shiryaev, E.V. Karaksina, T.V. Kotereva, A.P. Velmuzhov, M.V. Sukhanov, M.F. Churbanov, Core-clad Pr^{3+} -doped Ga(In)GeAsSe glass fibers for mid-IR radiation sources, J. Non-Cryst. Solids 537 (2020) 120026
[82] L. Sojka, Z. Tang, D. Jayasuriya, M. Shen, J. Nunes, D. Furniss, M. Farries, T.M. Benson, A.B. Seddon, S. Sujecki, Milliwatt-level spontaneous emission across the 3.5–8 μm spectral region from Pr^{3+} doped selenide chalcogenide fiber pumped with a laser diode, Appl. Sci. 10 (2020) 539
[83] J. Ari, F. Starecki, C. Boussard-Plédel, Y. Ledemi, Y. Messaddeq, J.-L. Doualan, A. Braud, B. Bureau, V. Nazabal, Co-doped Dy^{3+} and Pr^{3+} $Ga_5Ge_{20}Sb_{10}S_{65}$ fibers for mid-infrared broad emission, Opt. Lett. 43 (2018) 2893-96
[84] L. Sojka, Z. Tang, D. Jayasuriya, M. Shen, D. Furniss, E. Barney, T.M. Benson, A.B. Seddon, S. Sujecki, Ultra-broadband mid-infrared emission from a Pr^{3+}/Dy^{3+} co-doped selenide-chalcogenide glass fiber spectrally shaped by varying the pumping arrangement, Opt. Mater. Express 9 (2019) 2291-306
[85] J. Hu, C. R. Menyuk, C. Wei, L. B. Shaw, J. S. Sanghera, I. D. Aggarwal, Highly efficient cascaded amplification using Pr^{3+}-doped mid-infrared chalcogenide fiber amplifiers, Ot. Lett. 40 (2015) 3687-690
[86] M. Shen, D. Furniss, M. Farries, D. Jayasuriya, Z. Tang, L. Sojka, S. Sujecki, T. M. Benson, A. B. Seddon, Experimental observation of gain in a resonantly pumped Pr^{3+}-doped chalcogenide glass mid-infrared fibre amplifier notwithstanding the signal excited-state absorption, Scient. Rep. 9 (2019) 11426
[87] M. C. Falconi, G. Palma, R. Chahal, F. Starecki, V. Nazabal, J. Troles, J.L. Adam, S. Taccheo, M. Ferrari, F. Prudenzano, Dysprosium-Doped Chalcogenide Master Oscillator Power Amplifier (MOPA) for Mid-IR Emission, J. Lightw. Technol. 35 (2017) 265-273
[88] V.S. Shiryaev, M.V. Sukhanov, A.P. Velmuzhov, E.V. Karaksina, T.V. Kotereva, G.E. Snopatin, B.I. Denker, B.I. Galagan, S.E. Sverchkov, V.V. Koltashev, V.G. Plotnichenko, Core-clad terbium doped chalcogenide glass fiber with laser action at 5.38 μm, J. Non-Cryst. Solids 567 (2021)120939
[89] J. J. Nunes, Ł. Sojka, R. W. Crane, D. Furniss, Z. Q. Tang, D. Mabwa, B. Xiao, T. M. Benson, M. Farries, N. Kalfagiannis, E. Barney, S. Phang, A. B. Seddon, S. Sujecki, Room temperature mid-infrared fiber lasing beyond 5 μm in chalcogenide glass small-core step index fiber, Opt. Lett 46 (2021) 3504-507
[90] F. Starecki, F. Charpentier, J.L. Doualan, L. Quetel, K. Michel, R. Chahal, J. Troles, B. Bureau, A. Braud, P. Camy, V. Moizan, V. Nazabal, Mid-IR optical sensor for CO_2

detection based on fluorescence absorbance of Dy^{3+}: $Ga_5Ge_{20}Sb_{10}S_{65}$ fibers, Sensors Actu. B : Chem. 207 (2015) 518-25
[91] A.L. Pelé, A. Braud, J.L. Doualan, F. Starecki, V. Nazabal, R. Chahal, C. Boussard-Plédel, B. Bureau, R. Moncorgé, P. Camy, Dy^{3+} doped GeGaSbS fluorescent fiber at 4.4 µm for optical gas sensing: Comparison of simulation and experiment, Opt. Mater. 61 (2016) 37-44
[92] A.L. Pelé, A. Braud, J.L. Doualan, R. Chahal, V. Nazabal, C. Boussard-Plédel, B. Bureau, R. Moncorgé, P. Camy, Wavelength conversion in Er^{3+} doped chalcogenide fibers for optical gas sensors, Opt. Express 23 (2015) 4163-172
[93] F. Starecki, A. Braud, J.L. Doualan, J. Ari, C. Boussard-Plédel, K. Michel, V. Nazabal, P. Camy, All-optical carbon dioxide remote sensing using rare earth doped chalcogenide fibers, Opt. Lasers Engin. 122 (2019) 328-34
[94] H. Lin, Z. Luo, T. Gu, L.C. Kimerling, K. Wada, A. Agarwal, J. Hu, Mid-infrared integrated photonics on silicon: A perspective. Nanophotonics 7 (2017) 85
[95] M. Ahmadi, L. Bodiou, W. Shi, S. LaRochelle, Comprehensive modeling and design of Raman lasers on SOI for mid-infrared application J. Lightw. Technol. 38 (2020) 4114-4123
[96] B. Kuyken, T. Ideguchi, S. Holzner, M. Yan, T.W Hänsch, J. Van Campenhout, S. Coen, F. Leo, R. Baets, G. Roelkens, N. Picqué, An octave-spanning mid-infrared frequency comb generated in a silicon nanophotonic wire waveguide. Nature communications, 6 (2015) 6310
[97] M.R. Billah, M. Blaicher, T. Hoose, P.I. Dietrich, P. Marin-Palomo, N. Lindenmann, A. Nesic, A. Hofmann, U. Troppenz, M. Moehrle, S. Randel, W. Freude, C. Koos, Hybrid integration of silicon photonics circuits and InP lasers by photonic wire bonding. Optica, 5 (2018) 876-883
[98] D. Liang, X. Huang, G. Kurczveil, M. Fiorentino, R. Beausoleil, Integrated finely tunable microring laser on silicon, Nature Photonics 10 (2016) 719-722
[99] Y. Xia, C. Qiu, X. Zhang, W. Gao, J. Shu, Q. Xu, Suspended Si ring resonator for mid-IR application, Optics Letters, 38 (2013) 1122-1124
[100] J.D. Bradley, M. Pollnau, Erbium- doped integrated waveguide amplifiers and lasers. Laser Photon. Rev. 5 (2011) 368-403
[101] N. Li, E.S. Magden, Z. Su, N. Singh, A. Ruocco, M. Xin, M. Byrd, P. T. Callahan, J. D. B. Bradley, C. Baiocco, D. Vermeulen, M. R. Watts, Broadband 2-µm emission on silicon chips: monolithically integrated Holmium lasers, Opt. Express 26 (2018) 2220-2230.
[102] N. Li, P. Purnawirman, Z. Su, E.S. Magden, P.T. Callahan, K. Shtyrkova, M. Xin, A. Ruocco, C. Baiocco, E.P. Ippen, F. X. Kärtner, J. D. B. Bradley, D. Vermeulen, M. R. Watts, High-power thulium lasers on a silicon photonics platform. Optics Letters 42 (2017) 1181-1184
[103] Z. Tu, J. Zhang, J. Rönn, C. Alonso-Ramos, X. Leroux, L. Vivien, Z. Sun, E. Cassan, Potential for sub-mm long erbium-doped composite silicon waveguide DFB lasers, Scientific Reports 10 (2020) 10878.
[104] V. Nazabal, P. Němec, Amorphous thin film deposition, in: J.D. Musgraves, J. Hu, L. Calvez (Eds), Handbook of Glass, Springer, 2019, pp 1293-1332
[105] J. Orava, T. Kohoutek, T. Wagner, Deposition techniques for chalcogenide thin films, in: J.L. Adam, X.H. Zhang (Eds), Chalcogenide glasses, preparation, properties and applications, Woodhead Pub. Ltd, Cambridge, 2014, pp. 265-309

[106] M. Martino, A.P. Caricato, M. Fernandez, G. Leggieri, A. Jha, M. Ferrari, M. Mattarelli, Pulsed laser deposition of active waveguides. Thin Solid Films 433 (2003), 39-44.
[107] A.P. Caricato, M. De Sario, M. Fernandez, G. Leggieri, A. Luches, M. Martino, F. Prudenzano, Pulsed laser deposition of materials for optoelectronic applications, Appl. Surf. Sci. 197-198 (2002) 458-462
[108] A.P. Caricato, M. De Sario, M. Fernandez, M. Ferrari, G. Leggieri, A. Luches, M. Martino, M. Montagna, F. Prudenzano, A. Jha, Chalcogenide glass thin film waveguides deposited by excimer laser ablation, Appl. Surf. Sci. 208 (2003) 632-637.
[109] M. De Sario, G. Leggieri, A. Luches, M. Martino, F. Prudenzano, A. Rizzo, Pulsed laser deposition of praseodymium-doped chalcogenide thin films, Appl. Surf. Sci. 186 (2002) 216-220
[110] P. Nemec, M. Frumar, B. Frumarova, M. Jelinek, J. Lancok, J. Jedelsky, Pulsed laser deposition of pure and praseodymium-doped Ge-Ga-Se amorphous chalcogenide films, Opt. Mater. 15 (2000) 191-197.
[111] L. Bodiou, F. Starecki, J. Lemaitre, V. Nazabal, J.L. Doualan, E. Baudet, R. Chahal, A. Gutierrez, Y. Dumeige I. Hardy, A. Braud, R. Soulard, P. Camy, P. Němec, G. Palma, F. Prudenzano, J. Charrier, Mid-infrared guided photoluminescence from integrated Pr^{3+}-doped selenide ridge waveguides, Opt. Mater. 75 (2018) 109-115
[112] G. Louvet, S. Normani, L. Bodiou, J. Gutwirth, J. Lemaitre, P. Pirasteh, J. L. Doualan, A. Benardais, Y. Ledemi, Y. Messaddeq, P. Němec, J. Charrier, V. Nazabal, Co-sputtered Pr^{3+}-doped Ga-Ge-Sb-Se active waveguides for mid-infrared operation. Opt. Expr. 28 (2020) 22511-523.
[113] V. Lyubin, M. Klebanov, B. Sfez, M. Veinger, R. Dror, R., I. Lyubina, R. Earth, Photoluminescence, photostructural transformations and photoinduced anisotropy in rare-earth-doped chalcogenide glassy films, J. Non-Cryst. Sol. 352 (2006) 1599-1601
[114] V. Nazabal, P. Nemec, J. Jedelsky, C. Duverger, J. Le Person, J.-L. Adam, M. Frumar, Dysprosium doped amorphous chalcogenide films prepared by pulsed laser deposition, Opt. Mater. 29 (2006) 273-8
[115] S. Yang, X. Wang, H. Guo, G. Dong, B. Peng, J. Qiu, R. Zhang, Y. Shi, Broadband near-infrared emission in Tm^{3+}-Dy^{3}+ codoped amorphous chalcohalide films fabricated by pulsed laser deposition, Opt. Expr. 19 (2011) 26529
[116] E.N. Borisov, V.B. Smirnov, A. Tverjanovich, Y.S. Tveryanovich, Deposition of Er^{3+} doped chalcogenide glass films by excimer laser ablation, J. Non-Cryst. Sol., 326-327 (2003) 316-319
[117] Z.G. Ivanova, K. Koughia, D. Tonchev, J.C. Pivin, S.O. Kasap, Photoluminescence in Er-implanted amorphous Ge-S-Ga thin films, J. Optoelectron. Adv. Mater. 7 (2005) 1271-76.
[118] Z.G. Ivanova, K. Koughia, Z. Aneva, D. Tonchev, V. Vassilev, S.O. Kasap, Photoluminescence of Er^{3+} ions in $(GeS_2)80$ (Ga_2S_3) 20 glasses J. Optoelectron. Adv. Mater. 7 (2005) 349-352
[119] T. Sabapathy, A. Ayiriveetil, A.K. Kar, S. Asokan, S.J. Beecher,Direct ultrafast laser written C-band waveguide amplifier in Er-doped chalcogenide glass, Opt. Mater. Expr. 2 (2012) 1556-1561
[120] K. Yan, K. Vu, R. Wang, R., S. Madden, Greater than 50% inversion in Erbium doped chalcogenide waveguides. Opt. Expr. 24 (2016) 23304-313

[121] K. Yan, K. Vu, Z. Yang, R. Wang, S. Debbarma, B. Luther-Davies, S. Madden, Emission properties of erbium-doped Ge-Ga-Se glasses, thin films and waveguides for laser amplifiers, Opt. Mater. Expr. 4 (2014) 464-475
[122] T. Imai, K. Maeda, M. Fujita, N. Saito, Photoluminescence properties of erbium- doped amorphous gallium- germanium- selenium films fabricated by RF sputtering, Phys. Status Sol. C 6 (2009) S106-9
[123] K. Yan, R. Wang, K. Vu, S. Madden, K. Belay, R. Elliman, B. Luther-Davies, Photoluminescence in Er-doped Ge-As-Se chalcogenide thin films, Opt. Mater. Expr. (2012) 1270-77
[124] K. Yan, K. Vu, S. Madden, Internal gain in Er-doped As_2S_3 chalcogenide planar waveguides, Opt. Lett. 40 (2015) 796-99
[125] C. Vigreux-Bercovici, A Pradel, A. Fuchs, J. Fick, Effect of annealing on the photoluminescence in sputtered films of Er-doped chalcogenide glasses, Phys. Chem. Glasses - Eur. J. Glass Sci. Technol. B 47 (2006) 162-66
[126] J. Fick, É. J. Knystautas, A. Villeneuve, F. Schiettekatte, S. Roorda, K.A. Richardson, High photoluminescence in erbium-doped chalcogenide thin films, J. Non-Cryst. Solids 272 (2000) 200-8
[127] J.A. Frantz, L.B. Shaw, J.S. Sanghera, I.D. Aggarwal, Waveguide amplifiers in sputtered films of Er^{3+}-doped gallium lanthanum sulfide glass, Opt. Expr., 14 (2006) 1797-1803
[128] J. A. Frantz, L. B. Shaw, J. D. Myers, K. J. Ewing, J. S. Sanghera, Mid-IR Emission in Erbium-Doped Gallium Lanthanum Sulfide Glass Integrated Optic Waveguides, IEEE Photonics Society Summer Topical Meeting Series (2014) 49-50
[129] P.K. Dwivedi, Y.W. Sun, Y.Y. Tsui, D. Tonchev, M. Munzar, K. Koughia, C.J. Haugen, R.G. DeCorby, J.N. McMullin, S.O. Kasap, Rare-earth doped chalcogenide thin films fabricated by pulsed laser deposition, Appl. Surf. Sci. 248 (2005) 376-380
[130] V. Nazabal, P. Nemec, A.M. Jurdyc, S. Zhang, F. Charpentier, H. Lhermite, J. Charrier, J.P. Guin, A. Moréac, M. Frumar, J.L. Adam, Optical waveguide based on amorphous Er^{3+}-doped GaGeSbS(Se) pulsed-laser-deposited thin films, Thin Solid Films 518 (2010) 4941-4947
[131] S. Ramachandran, S.G. Bishop, Excitation of Er^{3+} emission by host glass absorption in sputtered films of Er-doped $Ge_{10}As_{40}Se_{25}S_{25}$ glass, Appl. Phys. Lett. 73 (1998) 3196-98
[132] A. Polman, Erbium implanted thin film photonic materials, J. Appl. Phys. 82 (1997) 1-39
[133] J.A. Frantz, J.S. Sanghera, L.B. Shaw, G. Villalobos, I.D. Aggarwal, D.W. Hewak, Sputtered films of Er^{3+}-doped gallium lanthanum sulfide glass. Mater. Lett. 60 (2006) 1350-1353
[134] A.K. Mairaj, A.M. Chardon, D.P. Shepherd, D.W. Hewak, Laser performance and spectroscopic analysis of optically written channel waveguides in neodymium-doped gallium lanthanum sulphide glass, IEEE J. Sel. Top. Quantum Electron. 8 (2002) 1381-1388
[135] S. Normani, G. Louvet, E. Baudet, M. Bouška, J. Gutwirth, F. Starecki, J.L. Doualan, Y. Ledemi, Y. Messaddeq, J.L. Adam, P. Němec, V. Nazabal, Comparative study of Er^{3+}-doped Ga-Ge-Sb-S thin films fabricated by sputtering and pulsed laser deposition. Scientific Reports 10 (2020) 7997

[136] G. Palma, P. Bia, L. Mescia, T. Yano, V. Nazabal, J. Taguchi, A. Moréac, F. Prudenzano, Design of fiber coupled Er^{3+}:chalcogenide microsphere amplifier via particle swarm optimization algorithm, Opt. Engin. 53 (2014) 071805_1-8
[137] F. Al Tal, C. Dimas, J. Hu, A. Agarwal, L.C. Kimerling, Simulation of an erbium-doped chalcogenide micro-disk mid-infrared laser source, Opt. Expr. 19 (2011) 11951-11962
[138] G. Palma, M.C. Falconi, F. Starecki, V. Nazabal, J. Ari, L. Bodiou, J. Charrier, Y. Dumeige, E. Baudet, F. Prudenzano, Design of praseodymium-doped chalcogenide micro-disk emitting at 4.7 μm, Opt. Expr. 25 (2017) 7014-7030
[139] L. Bodiou, Y. Dumeige, S. Normani, G. Louvet, P. Němec, V. Nazabal, J. Charrier, Design of a multimode interferometer-based mid-infrared multispecies gas sensor, IEEE Sensors J. 20 (2020) 13426-13435